Modeling And Simulation of Future Multi-User Communication System Including Capacity-Driven Array Synthesis And Beamforming

Gopika Sudhakaran

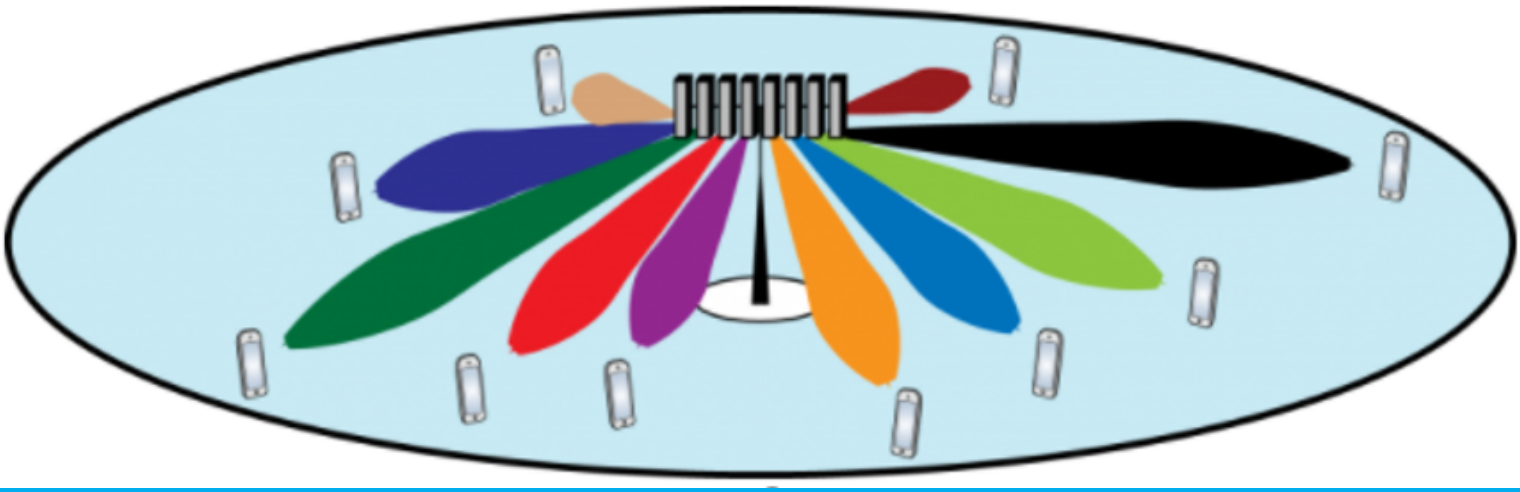

TU Delft

Modeling And Simulation of Future Multi-User Communication System Including Capacity-Driven Array Synthesis And Beamforming

by

Gopika Sudhakaran

to obtain the degree of Master of Science
at the Delft University of Technology

Student number: 5133424
Project duration: Dec 1, 2020 – Sept 1, 2021
Thesis committee:

Prof. DSc. A. Yarovoy,	Professor, Chairman Microwave Sensing, Signals and Systems
Dr. Yanki Aslan,	Assistant Professor, Microwave Sensing, Signals and Systems
Prof. Dr. Remco Litjens,	Associate Professor, Network Architecture and Services

TU Delft

Preface

Gopika Sudhakaran
Delft, August 2021

> "Success is no accident. It is hard work, perseverance, learning, studying, sacrifice and most of all, love of what you are doing or learning to do." -Pele

The inspiration for this research work has arisen from my passion for wireless communication technology. As the world progresses further towards achieving efficient connectivity and network for all, there is a growing need to contribute towards achieving this goal.

The completion of this thesis would have been impossible without the guidance and support from the faculty members and colleagues of Delft University of Technology. Firstly, I would like to take this opportunity to thank Prof. Alexander Yarovoy for giving me this opportunity to work with Microwave Sensing, Signals and Systems research group for my extra project and thesis. I am grateful to you for all the courses you have taught that helped me strengthen my fundamentals and kindle my interest in Antenna Systems and Electromagnetics.

I express my sincere gratitude towards my daily supervisor, Dr.Yanki Aslan for his constant advice and support in the formulation of the thesis goals and for helping me to achieve them. I would also like to thank Dr. Jan Puskely along with Dr. Yanki Aslan and Pascal Aubry for giving me the opportunity for practical experience of calibration of phased array antennas. I learned a lot during this project about beamforming and about conducting real-time antenna measurements.

I take this opportunity to specially thank Dr. Siavash Safapour of the University of Twente for extending his help regarding the modeling of the system and understanding of signal processing concepts. I would also like to thank Dr. Nitin Jonathan Myers for sharing his knowledge on signal processing for communications.

I would like to extend my thanks to Prof. Remco Litjens for instilling in me the interest in telecommunication during the fundamentals of wireless communication course.

Immense gratitude to MSc. Tworit Dash for our fruitful discussions on Antenna Theory, Electromagnetics, and implementation in MATLAB.

Finally, I would like to thank my parents and friends for their constant encouragement and support throughout the thesis.

Abstract

With the increasing demand for network services and a growing number of users, 5G communication systems have stringent requirements to fulfill. Due to this reason, 5G systems should employ capacity-oriented base station antenna arrays and beamforming techniques. In this regard, multi-beam antenna systems have gained immense attention. Currently, there is a missing link between antenna engineering and communication system design. Traditionally, antenna array design focused on optimizing free space propagation parameters like gain, directivity, sidelobe levels, etc. However, in order to achieve maximum network capacity, antenna array and beamforming techniques should consider a realistic system model and propagation environment. In this thesis work, we bridge the gap between antenna engineering and communication system design by proposing a multi-user communication system model that considers channel modeling, modulation, and RF aspects. Further, we use this model to assess the user performance in terms of Error Vector Magnitude (EVM) and Bit Error Rate (BER) for various base station antenna configurations and user positions. The results obtained showed that using an irregular antenna array at the base station with 64 elements shows an improvement in the performance of the users. With the presented simulation results, the system engineers can design efficient antenna arrays at the base station to achieve good performance on the millimeter-wave frequency bands.

Contents

List of Figures

List of Tables

1 Introduction

1.1. Background And Motivation

The fifth generation wireless communication system promises enhanced mobile broadband, ultra-reliable, and low latency communication. The key technologies that enable this feature include spatial-division-multiple-access(SDMA) and massive MIMO. In SDMA, multiple narrow beams are transmitted simultaneously towards different users[10]. The SDMA and antenna technology are closely linked to one another. Unlike the older generations of cellular networks where sector antennas were in use, in 4G and beyond multi-user MIMO(MU-MIMO) is widely used [11]. Their efficiency is more obvious in a multipath propagation context [12]. Spatial multiplexing can provide significantly higher peak data rates, spectrum efficiency, and improved system capacity[13]. However, the quality-of-service(QoS) for such systems are primarily constricted by the interference experienced by the users, which is very much dependent on the correlation amongst the users. The inter-user interference can be mitigated with the help of linear precoding techniques at the transmitter, such as the zero-forcing (ZF) precoding.

Initially, massive multiple-input-multiple-output (mMIMO) was introduced as an asymptotic concept where the base station(BS) antennas are increased to infinity. This theoretical assumption has helped to draw interesting conclusions such as the effect of noise, fast fading and some kind of interference and hardware impairments tend to vanish when averaged over infinitely many antennas [14]. Practically, the number of antenna elements considered starts from 64 and is expected to go up to 256. This results in a very large array gain and an improved energy efficiency since the entire energy can be directed to a particular space. The millimeter wave(mmWave) bands allow placing a large number of antenna elements in a compact structure. Recently, a lot of research work focuses on using mmWave bands due to their potential to support higher data rates and larger bandwidth [15]. However, mmWave massive MIMO poses several challenges. At these frequencies, the signals experience greater attenuation and hence results in increased path loss. Therefore, a high beamforming gain is required to compensate for the increased path loss. Another challenge is the hardware complexity for large arrays. Each antenna would require a dedicated Radio Frequency (RF) chain and mixed analog-digital equipment for beamforming [16]. This motivates the use of hybrid beamforming architecture, in which the number of RF chains and mixed analog devices is considerably reduced. As a result, it provides considerable hardware reduction and power-efficient solutions.

MIMO coupled with orthogonal- frequency-division-multiplexing(OFDM) is a powerful combination to achieve higher spectral efficiency. OFDM removes the inter-symbol interference(ISI) in frequency selective channels by transforming a wideband channel into numerous flat subchannels [17]. Moreover, with OFDM, the equalization complexity is reduced drastically since equalization is done in the frequency domain. MIMO-OFDM can take advantage of both spatial and frequency diversity while providing high data rates [18]. This combination proves to be of great advantage in massive MIMO context since OFDM can support more number of antennas and large bandwidth [19].

In order to achieve maximum throughput and capacity, the future communication system should carefully consider all the above mentioned technologies. Until recent times, antenna designers were focusing only on optimizing free space parameters such as half-power beamwidth, sidelobe level, gain, etc. While this is true in traditional communications and radars systems, the signal-to-noise ratio(SNR) enhancement in multi-antenna-based multi-user systems is achieved by spatially distributing the power constructively to utilize the multipath environment [20]. Hence, there is a growing need for antenna and beamforming techniques to consider realistic system models and propagation environments.

1.2. Literature Review

Over The Air measurements have been used in the telecommunication industry since the time of 2G. They were widely used to assess the performance of the radiation from the user equipment(UE). In several cases, it is claimed that OTA is the only instance for objective RF systems evaluation [21]. A number of authors have recognized this method for testing of the massive MIMO systems for 5G [1][22][23][24]. Antennas have always been measured in the anechoic chamber. However, with the onset of 4G, it was required to generate identical independently distributed channels(i.i.d). These were unable to create in an anechoic chamber since there was no delay-spread due to multipath. Therefore, a reverberation chamber that can emulate Rich Isotropic Multipath (RIMP) was proposed. As we move towards mmWave antennas for 5G, the scenario is different. At these frequencies, the multipath effect is reduced, and the transmission will largely depend on Line-Of-Sight(LoS) or dominant reflected or diffracted paths [1]. Hence, 5G systems are equipped with steerable beams which are assigned to each mobile user. Such test cases are suitable to be conducted in the anechoic chamber.

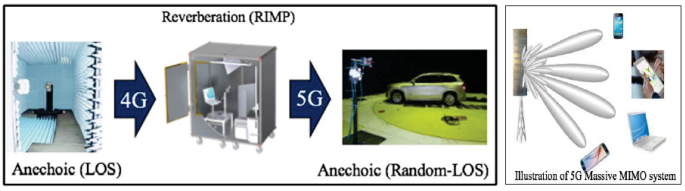

Figure 1.1: Figure showing how OTA testing has evolved from 3G to 5G (Adapted from [1])

Although some studies, such as [25], consider two extreme channel conditions (pure LoS vs. very rich scattering) and claim that any propagation model is likely to provide a performance (statistically) in between, such an assumption is, in general, not realistic. Besides, it is very important for the system designers to predict the performance of the overall network under real application scenarios before implementing each component. Moreover, such predictions can be very useful to improve the overall system performance by optimizing the design of each component (particularly the base station antenna array in our case). This can only be done via system-level simulations that rely on physically meaningful and computationally efficient methods characterizing the wireless channel, modulation, beamforming, and propagation scenarios.

This literature study gives an overview of the current channel, propagation models, and system simulators developed by different academic/industrial institutions for the 5G Multi-User MIMO system. Further, the existing MATLAB models are explored, which can be used in integration with the existing models to propose a new design. In the following section, we will discuss the existing channel and propagation models and then in a broader perspective, we will discuss the system-level simulators that are available.

1. Channel And Propagation Models
2. System Level Simulators

1.2.1. Channel And Propagation Models

To develop capacity-oriented MIMO models, it is necessary to have an accurate representation of the channel which is capable of including all the propagation mechanisms. There are several ways to group the channel models-physical and analytical, time-invariant and time-varying, narrowband and wideband channel models, etc. From a broader perspective, there are two types of channel models available in the literature-Stochastic and deterministic channel models [26]. The stochastic models compute propagation parameters like delay, angle of arrival, angle of departure, etc. based on parametric models which utilize known probability density functions. These models can be adapted to various scenarios mathematically and are less accurate. Whereas, deterministic models compute them accurately by solving Maxwell's equation or other propagation equations. However, such models are computationally very complex [27]. Hybrid models are also available, such as QuaDRiGa [28], which is a deterministic based stochastic channel model.

Examples of stochastic models include the 3GPP(3rd Generation Partnership Project) spatial channel model [29], Winner II [30], correlation-based stochastic models (CBSMs)[31], geometry-based stochastic channel models [32][33] where scatterers are placed in a random fashion according to certain probability distribution, Kronecker-based stochastic model (KBSM) [34], etc. In their recent works, [20],[35] the authors used two different channel models- International Mobile Telecommunications-Advanced (IMT-A) based NLoS(Non-Line-of-Sight) Urban Microcell and 3GPP Rural Macrocell Path Loss Models along with QuaDRiGa for an optimized MIMO phased array design. They bring about an innovative array design by taking into account the whole propagation scenario and characteristics of the environment. In this research, they define communication-link quality based on the computation of time domain Green's Function with the help of QuaDRiGa tool. Finally, a capacity-driven antenna array model is proposed which is compared with the traditional array design. It considers the optimization of clustered architecture for array design while considering the channel aspects. A sum-rate capacity and average directivity were measured for these models and the achieved results are reported. Finally, they compare the BER obtained using both models. By incorporating the channel model into the antenna array synthesis, this study clearly shows the high potential of a multidisciplinary system-level study for capacity improvement.

Another alternative to 3GPP spatial channel model is the NYUSIM channel models for 5G wireless Communications [36]. This simulation tool is developed on a statistical spatial channel model for mmWave applications. It provides accurate channel impulse responses in both time, space domain and also gives realistic signal levels at a wide range of frequencies. The model is created based on the mmWave measurements conducted in New York City [37]. It is also argued in [36] that NYUSIM produced more realistic simulations than 3GPP models. An example of a MU-MIMO system developed using the NYUSIM channel model is explained in [38]. A simple signal model is developed for two types of precoders: Zero Forcing and Conjugate Beam-forming. Channel parameters were obtained from the simulator and later a performance assessment based on the bit error rate for both

precoding strategies is mentioned. However, this model assumes that we have a perfect knowledge of channel state information at the base station and receivers.

Deterministic models include ray-tracing (RT) model [39], ray-launching (RL) model [40], and map-based model [41]. Ray-tracing is majorly used for channel characterization in indoor environments since it alleviates site-specific measurement campaigns. The electromagnetic wave is sent from the transmitter (TX) in RT modeling, which is presented as a series of rays based on geometric optics (GO) and uniform diffraction theory (UTD). This model includes the geometric features efficiently, hence it is faster and less expensive compared to the measurement campaign methods. However, the RT model depends heavily on various factors such as the environment, the objects present, and the continual angular dimension of ray launching (RL) [42]. This technique has been used in various research works to predict the propagation scenarios to evaluate the performance of millimeter waves MIMO systems [42][43][44]. The RT algorithm used in [42] consists of two stages. Firstly, visibility algorithm is used which creates a hierarchical database of the surrounding objects, and its visibility relation which is used to trace the real paths. The second step is the field computation process. Transmission losses are computed based on Fresnel's coefficients, and diffraction coefficients are calculated using Geometric Theory of Diffraction (GTD). Then the total electric field is calculated by [42, Eq. 1]. With these parameters, different beamforming solutions were investigated. In [43] and [44], the authors investigated the impact of forming a single-(multi-) lobe beam towards the strongest multipath component(s) of a user on the SINR performance. These studies clearly highlight the strong connectivity between the approach to antenna beamforming and the propagation environment in which it is placed.
In summary, the characteristics of the two widely used channel simulators discussed in this section are summarized in Table 1.1.

Simulator	Features
QuaDRiGa [45]	• Deterministic and statistical based channel model • Different environment scenarios available-Indoor office, Rural Macrocell, Urban Macrocell and Urban Microcell • Multi-frequency simulations (carrier frequencies from 500MHz to 100GHz) • varying speed for UE
NYUSIM [37]	• Statistical based channel model • Easy user interface • Frequency simulations for carrier frequencies from 2GHz to 73GHz • Available for various outdoor environments-urban microcell(UMi), urbanmacrocell(UMa), and rural macrocell(RMa) • Produces very accurate channel impulse response and signal levels

Table 1.1: Channel simulators

1.2.2. System Level Simulators

In this regard, we know that a complete 5G system development would involve consideration of a wide range of factors like physical layer aspects, access control, bandwidth allocation, etc. which can be managed easier with the help of simulators. Due to the complexities involved in developing such an integrated simulator that considers all the factors, the currently available ones may consider a subset of these factors [26]. Table 1.2 which is an extension of the list provided in [26], summarizes the most widely used 5G channel simulators and their characteristics.

Simulator	Features
Wireless Simulator Evolution (WiSE) [46]	• System level simulations of 5G networks for multitier orientations • Source code is available for simulation
[47]	• Can be used for heterogeneous networks • Simultaneous over numerous access technologies • Open functional interfaces
[48]	• mmWave transmission • User scheduling
Vienna 5G system Simulators[49]	• Large scale 5G simulations possible with hundreds of nodes in parallel • Multi-tier orientation • For mm-wave frequencies and beyond
GTEC 5G Simulator	• 5G link level simulations • Transceiver implementation
RANPLAN	• Supports AR/VR • Radio Network Planning • simulations for 100 MHz to 70 GHz
5G Toolbox by MATLAB	• 5G link level simulations • signal generation • channel modeling
[50][51][52]	• based on circuit theory of communication • incorporates mutual coupling and multipath effects • Flexible frequency
ns-3 simulator [48]	• Able to incorporate real measurements or ray tracing data • Includes detailed statistical channel models • User scheduling

Table 1.2: Examples of widely used 5G simulators with their main features

1.2.3. Overview Of MATLAB Models

MATLAB along with Simulink is a promising platform to design and develop a MU-MIMO beamforming system for 5G applications. The recently released 5G toolbox brings forth standard-compliant functions and examples for design, simulation and performance evaluation of 5G New Radio(5G NR) systems [53]. The supplementary toolboxes that can help in the complete design of the communication system include the Phased Array System Toolbox, Antenna Toolbox, RF Toolbox, Communications Toolbox, etc. In this section, we explore the various examples that can be used to develop a MU-MIMO System for 5G and their features are summarized in Table 1.3.

A. Massive MIMO Hybrid Beamforming

This MATLAB example showcases the use of hybrid beamforming at the transmit end of a massive MIMO system designed for both multi-user and single-user applications. Figure 1.2 presents a functional model of the system. The base station and the receiver side antenna elements can be set. It uses full channel sounding to determine the channel state information (CSI) at the transmitter. There are two channel models available: One Ring scatterer model as well as MIMO flat fading model(narrowband model). One ring scatterer model employs ray-tracing approximations with a number of scatterers which are placed in a circle around the receiver [54]. The 3D radiation pattern is obtained for both the transmit side and the receive side antennas. Apart from that, the analysis of the system is done based on the QoS metrics calculated- EVM and BER.

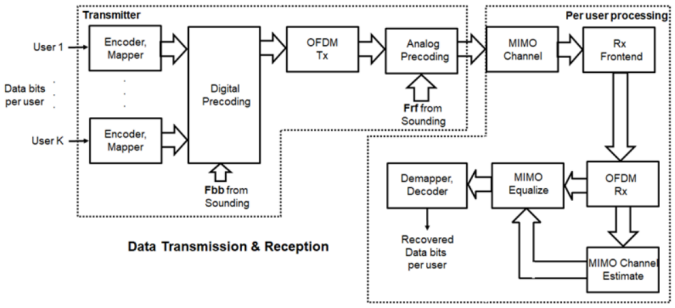

Figure 1.2: Data transmission and reception model(Adapted from [2])

B. Hybrid MIMO Beamforming With QSHB And HBPS Algorithms

In this example, a Simulink model of MIMO Hybrid beamforming is proposed. It consists of four main parts: MIMO Transmitter, MIMO receiver, MIMO channel, and weights calculation for the beamformer. The model compares two hybrid beamforming algorithms: Quantized Sparse Hybrid Beamforming (QSHB) and Hybrid Beamforming with Peak Search (HBPS). The results are verified by plotting the constellation diagram and comparing the received symbol with the source constellation. Figure 1.3 gives the Simulink model of this example.

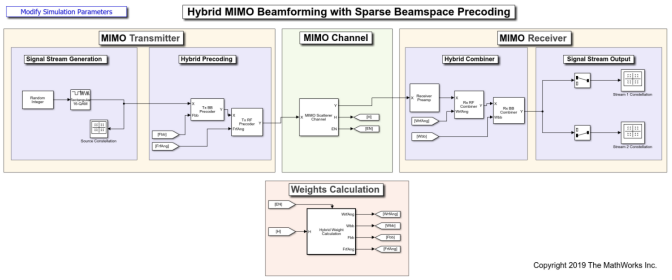

Figure 1.3: Hybrid beamforming MIMO with sparse beam-space precoding(Adapted from [3])

C. Modeling An RF mmWave Transmitter With Hybrid Beamforming

This example presents a system-level model of 66 GHz QPSK RF transmit-receive system consisting of 32 element array(4 sub-arrays of 8 patch element array). Figure 1.4 gives a high-level model of this example. This model considers the transmit array radiation effects, RF imperfections(noise, antenna mutual coupling, non-linear effects), a narrowband receive array, and baseband receiver. A text message is sent from the transmitter over the channel, which is a simple free-space path loss model. It also corrects errors due to system impairments and message decoding. Apart from that, the model employs the MUSIC algorithm to estimate the beamforming elevation and azimuth angles. Hybrid beamforming weights are calculated by the MVDR algorithm(Minimum Variance Distortionless Response). Finally, at the receiver, the message is demodulated and the EVM and MER(Modulation Error Ratio) are displayed.

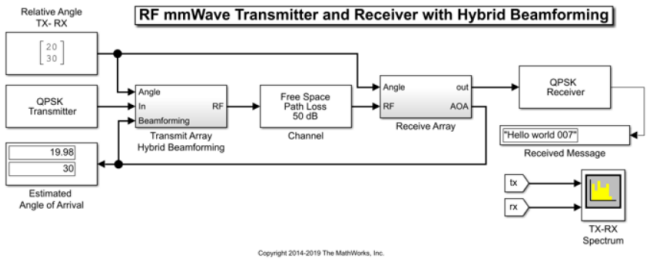

Figure 1.4: System model with mmWave transmitter and Hybrid Beamforming (Adapted from [4])

D. 802.11ac Multi-User MIMO Precoding With WINNER II Channel Model

This example demonstrates transmit-receive processing for IEEE 802.11ac for multi-user scenario over a WINNER II channel model [55]. We can have up to 4 users and 8 transmit antennas for 802.11ac. There is a specific time slot for each user, and the scheduler chooses the smaller packets which are ready to be transmitted to other users. A precoding method is then employed in order to be able to transmit multiple streams(maximum 8). Individually, the users would transmit their CSI to the beamformer, and based on this, the precoding matrix is calculated. A random set of bits are used as the data sent over the channel for each user. This data is recovered at the receiver side and assessment of the system is done based on BER and EVM.

E. MIMO-OFDM Precoding With Phased Arrays

This example presents an asymmetric MIMO OFDM system for a single user(one base station communicating with one user). This system is capable of producing 16 independent streams with the help of antenna elements at the base station. The maximum allowable number of transmitter antennas at the base station is 1024 and for the receiver, it is 32. This data is transmitted over a spatial channel model like WINNER II and also scattering based channel model. The system performance is measured with BER, EVM, and MER.

Example Models	Features						
	Beamforming	**frequency**	**Modulation**	**Antenna Configuration**	**Users**	**Channel model**	**Metrics**
Massive MIMO Hybrid Beamforming [2]	Hybrid,Precoding: beam steering	28GHz	OFDM(QPSK;QAM)	Transmit & Receive: ULA/URA	Multi-user	Single bounce RT model	BER,EVM
Hybrid MIMO Beamforming With QSHB And HBPS Algorithms [3]	Hybrid, Precoding: beam steering	28GHz	QAM	Transmit & Receive: ULA/URA	Single	Single bounce RT model	Constellation diagram
Modeling An RF mmWave Transmitter With Hybrid Beamforming [4]	Hybrid, MVDR Beamformer	66GHz	QPSK	Transmit:URA, Receive: 2 orthogonal linear array	Single	Free space path loss	EVM,MER
802.11ac MU MIMO Precoding With WINNER II Channel [56]	MMSE (minimum mean squared error) precoder or Zero-forcing precoder	5GHz	QAM,QPSK	Transmitter: Uniform circular array(UCA) ,Receiver: ULA	Maximum Four	WINNER II	EVM,BER
MIMO-OFDM Precoding With Phased Arrays[57]	Digital,beem steering	4GHz	OFDM(QAM)	Transmit: URA/ULA, Receive:URA/ULA	single	WINNER II,Scattering	EVM,MER,BER

Table 1.3: Relevant MATLAB Models

1.3. Conclusion Of Literature Study

With the shift towards 5G communication technology, MU-MIMO systems have become an integral part. To facilitate maximum network capacity for 5G systems, antenna array and beamforming techniques should consider realistic channel and propagation models. Current research studies show there is a missing link between antenna engineering and the communication system, and there is a growing trend to bridge this gap by characterizing antenna arrays within the environment.

In this literature survey, a compact, high-level research on 5G channel models, propagation scenarios, and system-level models for MU-MIMO was conducted. However, a closer look at the literature reveals some shortcomings and gaps. Let us have a brief look at some of the key references discussed in sections 1.1, 1.2. (i)In [20], the authors propose a capacity-oriented array design using the 3GPP channel model and QuaDRiGa simulator. However, complete consideration of the communication system model with different modulation schemes and RF impediments is missing. Apart from that, the study is done below 6GHz where the multipath is rich and the mmWave scenario is not investigated. Furthermore, the mentioned approach examines the spatial diversity concept, yet some important system aspects such as the trade-off between array gain and the number of multipath channels used, the complexity of synchronization of the multipath signals, fairness among the users, etc. are missing. (ii)Previous research on ray-tracing revealed that its computational complexity is high. Moreover, it is a slow process, and the model is heavily site-specific which cannot be used for a generic study. (iii)Amongst the simulators, the network model proposed in [50][51][52] does not consider a realistic channel model. Besides, in [50], it uses co-simulation in MATLAB and EM simulation software, which can be time-consuming.

A more realistic channel modeling can be done in QuaDRiGa which can support multi-user, multi-antenna technologies as well as different environments. We can track the users in an evolving environment, which makes it easy to study the effect of the propagation environment on the performance of the system. An alternative model would be the statistical-based NYUSIM model [38] which has a well-designed user interface. We can easily select channel parameters and antenna properties in the GUI. However, due to its statistical nature, you cannot choose the positions of the user, which makes it difficult to assess the performance of the system.

A promising system-level simulator would be MATLAB which has various toolboxes like 5G Toolbox, Phased Array Toolbox, etc. that is suitable for the design and analysis of MU-MIMO systems. The MATLAB examples in 1.2.3(B), 1.2.3(C), and 1.2.3(E) are for single user scenarios and to extend it to a multi-user scenario might be complex. In model 1.2.3(D), there is an upper limit to the maximum number of users, which is 4. This would limit our exploration of study in terms of capacity. However, in model 1.2.3(A), we can define the number of users. Moreover, the flexibility in the antenna array design is an advantage. Hence, this is a suitable model for multi-user scenarios which

is designed at frequency 28GHz that we are interested in.

In this section, we have identified the advantages/disadvantages of different simulators and selected the most relevant and high-potential tools among them to be used in this thesis.

1.4. Aim Of Research And Novelties

The goals of the thesis are defined as follows:

1. To develop a 5G communication system model that includes modulation, channel, and possibly RF aspects in a compact system model with flexibility in simulation scenario (environment settings, user distribution, base station location, etc.).
2. Use the model to evaluate the performance of different antenna configurations and understand the trade-offs.

We propose a MATLAB model in line with these goals for the thesis. The MATLAB example in 1.2.3(A) will be extended to modify the antenna design for the base station and user equipment. The analysis can be done with the existing MIMO scatter-based channel model. Finally, the performance assessment will be done using EVM, BER measurements.

In this thesis, a complete system model for multi-user scenario and multi-beam antenna arrays at the base station has been developed. To our knowledge, this is the first time such a comprehensive model has been presented in the literature. With the developed model, a novel investigation of the impact of user location on the system performance is conducted. In a MU-MIMO system, interference is heavily dependent on the spatial correlation among the users. With this study, we determine the user position that achieves better performance. Another novel aspect includes the analysis of the antenna array size and topology on the system performance. These parameters influence the nature of beams assigned to the users and hence affect the overall performance.

1.5. Outline

The following is how the rest of the thesis is organized:

1. Chapter 2 gives an overview of the developed Multi-User MIMO system model and its components. The considered channel model, beamforming architecture, and precoding strategy are discussed in detail.
2. In Chapter 3, statistical analysis of the model is conducted. Different case studies are performed using the developed model and results are presented.
3. A summary of the thesis is given in Chapter 4. We conclude the thesis with the findings from the results, following which the future scope of the thesis work is outlined.

2

System Model

Traditionally, MIMO was intended for point-to-point communications. Over time, MIMO has been extended for multi-user scenarios. A multi-user MIMO (MU-MIMO) system consists of a base station with a large array of antennas that communicates with multiple users having single or multiple antennas. Such systems are known to improve the capacity and coverage of the future communication system. It facilitates the spatial sharing of the channels, which can be attained by using multiple hardware elements like antennas and filters. This way, such systems can provide high data rates without compromising the spectrum bandwidth and energy consumption.

In this chapter, we look into the extended MATLAB model in detail. The model considers a multi-user massive MIMO communication system with hybrid beamforming architecture at the transmitter. Channel sounding is implemented to get Channel state information(CSI) at the transmitter. Multiple data streams are OFDM modulated and transmitted from the users, which are received by simple digital receivers. The performance of this system is evaluated by the popular figures of merit-Bit Error Rate(BER) and Error Vector Magnitude(EVM).

MU-MIMO System Model

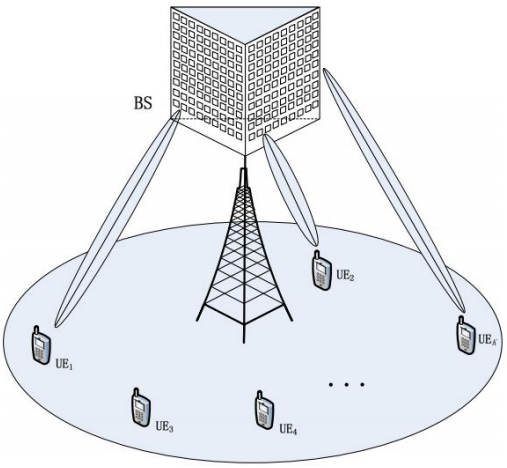

Figure 2.1: An illustration of Massive MU-MIMO system consisting of *M* BS antennas and *K* users in a cell [5]

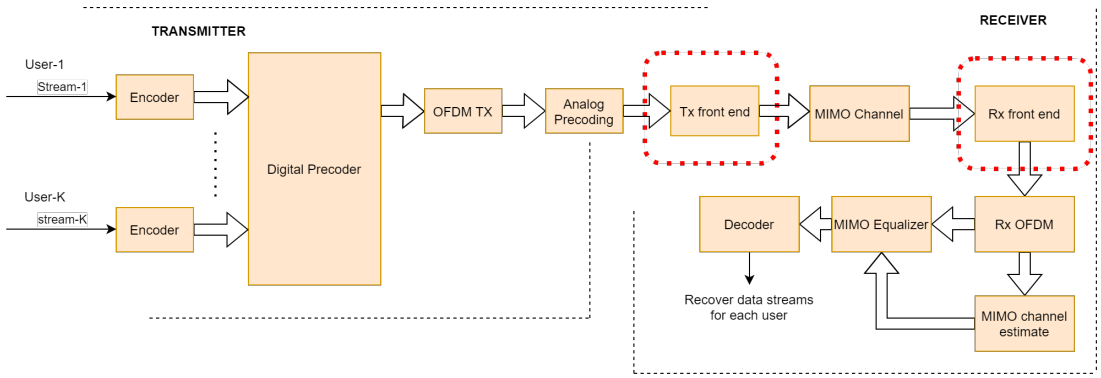

Figure 2.2: Multi-User downlink communication model(red blocks are modified for our study)[2]

A representation of the Massive MU-MIMO system is shown in Figure 2.1. This model considers a downlink MIMO-OFDM scenario in which a base station (BS) antenna array consists of M elements and users equipped with *L* antenna elements each. The BS serves *K* users ($K \leq M$) in a cell simultaneously by transmitting N_s data streams over *n* OFDM sub-carriers. N_s is upper limited by the lower number of antenna elements present in the BS, and the aggregate of all UE's antenna elements [58]. We assume a planar antenna array at the BS, while a linear antenna array is employed at the user side. Figure 2.2 shows the block diagram of the downlink MU communication system for the discussed MATLAB model. The highlighted red blocks are the ones that we modified for our study. Let us consider the scenario where the BS transmits a single data stream to each user. These streams are encoded using convolutional codes. In order to take advantage of the multipath during propagation, a spatially multiplexed system needs to have knowledge of the channel profiles. These profiles are called channel state information (CSI) which can be obtained by sounding the channel with a reference signal. Since the model employs the Frequency Division Duplex(FDD) mode, the BS broadcasts the pilot signals over all the *M* antenna elements to *K* users simultaneously over *n* OFDM subcarriers. The users estimate the channel from these pilots and the channel estimate is fed back to the BS, which is used to calculate the precoding matrices. This model assumes slow varying channel and perfect feedback from all the users, while it does not consider quantization or implementation delays. The channel model that is used for this system is similar to the 'One-Ring' model, which creates a NLoS propagation scenario with the presence of scatterers around each user. It takes into account the spatial locations of the transmit and receive array as well as the array geometry.

As we are focusing on mmWave communication system, we require a large antenna array at the base station. A large antenna array would mean an increase in the number of Radiofrequency(RF) chains for each antenna element. This results in higher costs and energy consumption. A more practical approach in such a case is to use hybrid transceivers, which use a combination of analog beamformers in the RF domain and digital beamformers in the baseband domain. In this way, we use fewer RF chains than the number of transmit antennas [58]. In this model, we consider the number of RF chains to be equal to the total sum of data streams that are assigned to each user. Further, we employ Joint Spatial Division and Multiplexing technique to obtain higher gains for the FDD system with the reduced requirement on channel state information at the transmitter(CSIT) [59]. Following this, the data transmission is configured. This step involves the generation of transmit bits, which are encoded using convolutional codes. Subsequently, the encoded data bits are mapped onto Quadrature Amplitude Modulation (QAM) symbols for each data stream, which is then mapped onto each RF chain. This is followed by applying baseband precoding weights to the mapped data symbols, after which OFDM modulation with pilot mapping is performed. Finally, this transmit signal

is multiplied with the analog precoding weights and sent across the same channel which was used for sounding to different users in the cell. At the receiver, these received signals are amplified by the front-end amplifiers. At this stage, thermal noise is also added. Further, the received signals are demodulated, and channel estimation is performed. Since we consider a wideband system, the channel response would experience a lot of fluctuations and equalization should be performed to have sufficient detection. The obtained CSI at the receiver is used for the soft decoding process and a convolutional decoder is used to recover the data bits at each user.

2.1. Channel Model

One Ring channel model is a popularly used ray tracing channel model for fixed wireless communication systems where the BS and the users are at a constant position. The BS is usually elevated and unhampered by the scatterers whereas the User Equipment (UE) is surrounded by local scatterers [6]. They are placed in a ring of radius *R* around the UE, as shown in Figure 2.3. In this system, we consider 100 scatterers around each UE. The radius *R* is dependent on the root-mean-square (RMS) delay spread of the channel. The main parameters of the model are the distance *D* between the transmitter and receiver, the scattering ring radius *R*, the angle of arrival Θ at the BS, and the geometrical configuration of transmit and receive antenna. With respect to the antenna elements, the incoming waves are within angles $[\Theta - \Delta, \Theta + \Delta]$ where Δ is the angular spread.

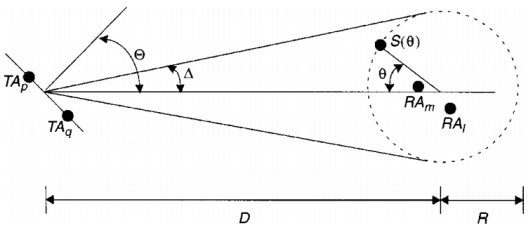

Figure 2.3: One-Ring Channel Model for a single UE (Adapted from [6])

The assumptions made in the model are as follows [60],[61]:

1. Each scatterer positioned at an angle θ to the receiver is described by an effective scatterer placed at the same angle on the scattering ring with center as the UE. Both the scatterers are uniformly distributed in θ. Let $S(\theta)$ be the effective scatterer located at an angle θ and $\phi(\theta)$ be the associated phase. $\phi(\theta)$ is characterized by the dielectric properties and radial displacement of the actual scatterer from the ring. Hence, all the rays impinging on the effective scatterer $S(\theta)$ would undergo a phase change $\phi(\theta)$. The phase change is uniformly distributed in $(-\pi, \pi]$, independent and identically distributed (i.i.d.) in θ.
2. The rays with single reflection alone are considered.
3. All the rays arrive at the receive antenna with the same power.

Let us consider that we have Q effective scatterers $S(\theta_q)$ with q=1,2...Q. The complex path gain between the base station element TA_p and the receive antenna RA_l is given as:

$$H_{l,p} = \frac{1}{\sqrt{2\pi}} \int_0^{2\pi} \frac{1}{\sqrt{Q}} \sum_{q=1}^{Q} \delta(\theta - \theta_q) exp\left\{-j\frac{2\pi}{\lambda}.(D_{TAp \to S(\theta)} + D_{S(\theta) \to R_{Al}}) + j\phi(\theta)\right\} d\theta \tag{2.1}$$

Here, $D_{X \to Y}$ is the distance from X object to Y object and λ is the associated wavelength. This way, the channel coefficients are calculated for the One-Ring model.

In this thesis work, we implemented an extended version to consider the scatterers placed in a spherical volume around the UE. These scatterers are placed randomly in a defined boundary which is the radius in X, Y and Z directions.

2.2. Hybrid Beamforming And Precoding

Massive MIMO systems experience two major problems:(i) a Large number of RF chains would be required, which results in higher cost and power consumption (ii)obtaining CSI between each transmit-receive antenna would utilize the majority of the spectral resources[58]. The concept of hybrid beamforming presents a potential solution to these problems, and it was first suggested in [62] and [63]. This model considers a reduced-dimensional baseband digital beamforming technique used along with a phase shifter network to decrease the number of required RF chains [64]. Figure 2.4 depicts the hybrid beamforming structure employed at the BS. It comprises a baseband digital precoder F_{BB} that generates N_s outputs after processing N_s data streams. These N_s outputs are upconverted to RF domain and the analog precoder F_{RF} maps them to *nTx* antenna elements. In a fully connected structure, every RF chain is linked to all antenna elements using adders, as shown in Figure 2.4. Such a system provides higher beamforming gain and beam agility at the cost of complexity.

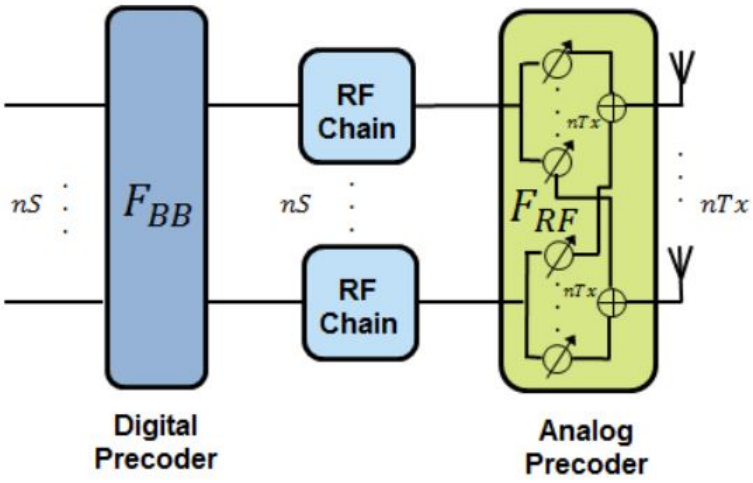

Figure 2.4: Fully connected hybrid beamforming block diagram(Adapted from [2])

Since we consider the system to work in FDD mode, high overhead of the feedback of CSI to the transmitter, poses to be a big challenge [65]. For FDD systems, the spacing between uplink and downlink frequencies are much larger than the coherence bandwidth[66]. As a consequence, the channel state information at the transmitter (CSIT) has to be provided by the users to the BS. Because of the massive MIMO scenario, feedback overhead would be larger, thus reducing the bandwidth efficiency of the system. There are various works in the literature that focuses on the reduction of the feedback overhead [67], [68]. One such technique is the Joint Spatial Division and Multiplexing(JSDM) which was first proposed in [68]. The primary goal of this method is to group the users that have similar covariance and also partition the beamforming in two stages. The first stage is that of a pre-beamformer where the analog beamforming is based on the average CSI, while the second stage is the digital beamforming adapted to instantaneous CSI, obtained following the pre-beamforming [58]. This way, JSDM naturally fits into the hybrid structure [59].

The analog beamformer utilizes the Block Diagonalization(BD) technique to suppress the inter-group interference [64] performed over the averaging of the channel matrix across subcarriers. For the sake of simplicity, in this model, we consider that each user belongs to its own group (grouping not performed). Let $H = [H_1, .., H_k]$ be the overall channel matrix [59]. The Channel vectors for each user is $H_k \in C^{M \times L}$, where *L* is the number of antennas at the receiver. Further, b is the number of RF chains and N_s is the number of data streams assigned for each user. In order to make the notations simpler, we are focusing on a fixed OFDM subcarrier. The received signal for all the served users is given by the following equation [59, Eq. 6]:

$$y = H^H V D + z \tag{2.2}$$

where *y* is the received signal $y \in C^K$,$V \in C^{M \times K}$ is the precoding matrix,$D \in C^K$ is the data stream vector and z is the Additive White Gaussian Noise (AWGN) with i.i.d. of zero mean and variance as one. The beamforming matrix is given by $v = F_{RF} \times F_{BB}$ where $F_{RF} = B$ is the pre-beamformer matrix(analog) of the dimension $M \times b$ and $F_{BB} = (P_1, \cdots P_k)$ is the baseband precoder matrix of dimension $b \times K$ for each user *K* which is computed based on the effective channel matrix $\tilde{H} = F_{RF} H$. The equation 2.2 can be expanded as:

$$y = \begin{bmatrix} y_1 \\ \vdots \\ y_k \end{bmatrix} \tag{2.3}$$

$$y = \begin{bmatrix} H_1^H B_1 P_1 d_1 + \sum_{k' \neq 1} H_1^H B_1 P_{k'} d_{k'} + z_1 \\ \vdots \\ H_K^H B_1 P_K d_K + \sum_{k' \neq K} H_K^H B_1 P_{k'} d_{k'} + z_K \end{bmatrix} \tag{2.4}$$

In order to eliminate the inter-user interference, we need to impose the below-mentioned condition in the BD algorithm:

$$H_k^H B_{k'} \approx 0 \, \forall \, k' \neq k \tag{2.5}$$

In the next section, we discuss in detail the BD approach.

Precoding

MU MIMO systems utilize the spatial dimension to make sure that the beams are formed in the direction of the user of interest. This is achieved by precoding the transmit signal at the BS. With precoding, the transmit signal is distributed over each antenna element at the BS to achieve beamforming of the signal towards the users [38]. The precoding weights can be computed from the knowledge of the channel that provides us with the information of constructive and destructive interferences of the beams in the form of complex gains associated with every transmit-receive antenna pair. There are two kinds of precoding: linear and non-linear. Linear precoding transmits data linearly and can achieve reasonable performance with lower complexity. Whereas, non-linear precoding techniques are complex but can attain higher capacity. Some examples of linear precoding include Maximum Ratio Transmission(MRT) [69], Zero-Forcing precoding(ZF) [18], Transmit Wiener precoding [70], Minimum Mean Square-Error(MMSE) [71] etc. On the other hand, Nonlinear precoding is based on the theory of Dirty Paper Coding (DPC).

In order to achieve better performance of the massive MU-MIMO systems, efficient multi-user interference cancellation is required. Hence, precoding techniques such as Zero-Forcing is often used for interference control. In this work, we apply a generalization of the fundamental ZF Beamforming technique called Block Diagonalization, which is used for the BS and UE equipped with multiple antennas [72]. The fundamental ZF technique is suitable for single-antenna users where it

completely diagonalizes the channel and cancels the inter-user interference. Conversely, if the user has multiple antennas, this solution may not produce the same results because the user can now coordinate the processing about its own receiver output. Moreover, if the antennas at the receiver have a strong spatial correlation, complete diagonalization will reduce the throughput [73].

As discussed earlier, let us consider the channel matrices of all users $H = [H_1^T, .., H_K^T]$ and the pre-beamforming matrix $B = [B_1, .., B_K]$. For generalized ZF precoding, HB should be block diagonal. An assumption made in this algorithm is that the number of BS antennas are to be larger than the total number of receive antennas. If $\tilde{H}_j = \left[H_1^T, \cdots, H_{j-1}^T, H_{j+1}^T, \cdots H_K^T\right]$ be the channel matrix of all user other than *j*, then the beamforming matrix of B_j should lie in the null space of $\tilde{H}_j$ for the zero interference condition. This condition is satisfied when the $rank\left(\tilde{H}_j\right) < M$. Now suppose, $\tilde{N}_j = rank\left(\tilde{H}_j\right) \leq L - L_j$, then the Singular Value Decomposition (SVD) can be obtained as :

$$\tilde{H}_j = \tilde{U}_j \tilde{\Sigma}_j \left[\tilde{V}_j^{(1)} \;\; \tilde{V}_j^{(0)}\right]^H \tag{2.6}$$

where $\tilde{V_j^{(1)}}$ represents the first $\tilde{N}_j$ right singular vectors and $\tilde{V_j^{(0)}}$ the last $M - \tilde{N}_j$ right singular vectors [72]. Hence, $\tilde{V_j^{(0)}}$ holds the orthonormal basis for the null space of unintended users $\tilde{H}_j$ and its columns forms the elements for the beamforming matrix B_j. In order to have maximum data rate transmission to user j, the pre-beamforming matrix can be calculated by the following:

$$B = \left[\tilde{V}_1^{(0)} \tilde{V}_1^{(1)} \;\; \cdots \tilde{V}_K^{(0)} \tilde{V}_K^{(1)}\right] \tag{2.7}$$

Hence, we now proceed with the calculation of the baseband precoder *P* which depends on the instantaneous channel statistics. For every subcarrier, we perform the SVD of the reduced effective channel for each user $\tilde{H}_k = B_k^H H_k$ in order to obtain the baseband precoder.

$$\tilde{H} = \bar{U}_j \bar{\Sigma}_j \bar{V}^H \tag{2.8}$$

where V represents the baseband precoding matrix, which is nothing but *P* in our case.

2.3. Conclusion

In this chapter, we discussed an extended MU-MIMO system simulator developed in MATLAB based on the model given in 1.2.3(A). We explored the different blocks of the communication model, out of which, we delved into the details of the channel model and the beamforming architecture. A complete NLoS channel model with scatterers arranged in one ring has been studied. Suitable beamforming and precoding techniques for the FDD system were discussed. Finally, the model considers all the main aspects of communication theory into account, in order to represent a realistic system environment.

3

Analysis Of The Model

This chapter includes the detailed statistical analysis of the model discussed in Chapter 2. To begin with, we will discuss the system specifications followed by case studies. Primarily, the case study revolves around the two different planar array topologies designed for the BS: i)Regular array and ii)Irregular array. We evaluate the performance of the users in terms of the BER and EVM for all the cases. In this thesis work, the following cases are investigated for each antenna array topology:

- Regular/Irregular planar array at BS
  1. Changing User position
     (a) Change of user range
     (b) Change of user azimuth
     (c) Change of user elevation
  2. Increasing the number of transmit elements

The above cases are performed with the extended One Ring channel model for different scattering environments to study the multipath effects. A comprehensive study of each case will be discussed in this chapter.

3.1. Model Specifications

A MU-MIMO communication model was developed for fifth generation wireless technology. Our system consists of two users located several meters away from the BS in a single cell. The maximum distance between the BS and users is taken to be 200 meters and the BS is assumed to be located at [0,0,0] in the Cartesian plane. The users' azimuth and elevation angles are defined within the range [-60 60]° and [-15 15]°, respectively. These values are considered in accordance with the 5G standards. A simple realization of the explained simulation is depicted in Figure 3.1. The definition of the coordinate system can be found in Appendix-A. For the BS, we consider two different topologies in our analysis-(i)Uniform Rectangular Array(URA) and (ii) Irregular antenna array designed for the mmWave frequency 28GHz. On the other hand, each user is equipped with a uniform linear array with 3 isotropic antenna elements.

This work focuses on the multi-user downlink scenario, where the BS sends a single data stream to each user. For most of the simulations, we keep the transmit power as a constant of 1 Watt since we are dealing with a theoretical study with the main focus on the effect of interference between

the users assessed based on EVM, BER, and not SNR. The data streams are encoded using convolutional codes and OFDM modulated before it is sent across a wideband channel. In this model, we consider 10 OFDM symbols in a single slot, and each symbol comprises 234 subcarriers. Every subcarrier carries baseband data which are independently modulated with Quadrature Amplitude Modulation. For most simulations, we use a 16-QAM modulation scheme. For the channel model, we have 100 scatterers placed randomly around each of the users in a sphere of radius R which is dependent on the user's range. With this channel, we simulate a complete NLoS scenario. A complete model parameter list is summarized in Table 3.1. Further, the system is used for conducting the statistical evaluation of performance in terms of BER and EVM by changing user positions, antenna array topology, and array size.

System Parameters	Values	
Antenna	**Base Station(gNodeB)**	
	No. of elements	64,256
	Topology	Regular, Irregular array
	Array element	Patch
	Element spacing	0.5 λ,0.6λ
	Position[x,y,z]	[0,0,0]
	User Equipment	
	No. of elements	3
	Topology	Linear array
	Array element	Isotropic antenna
	Element spacing	0.5 λ
	Position[x,y,z]	Variable
Channel	Number of scatterers	100
	Radius of ring	0.1*Range of User
OFDM Modulation	No. of subcarriers	234(based on [2])
	Cyclic prefix length	64(based on [2]))
	Subcarrier modulation	16-QAM
Others	No. of users	2
	Total no. of data streams	2
	Azimuth scan	[-60 60] deg.
	Elevation scan	[-15 15] deg.
	Maximum range of users from BS	200 meters
	Operational Frequency	28 GHz
	Noise Figure	6 dB(based on [2])
	Code Rate	1/3(based on [2])

Table 3.1: Important System Parameters

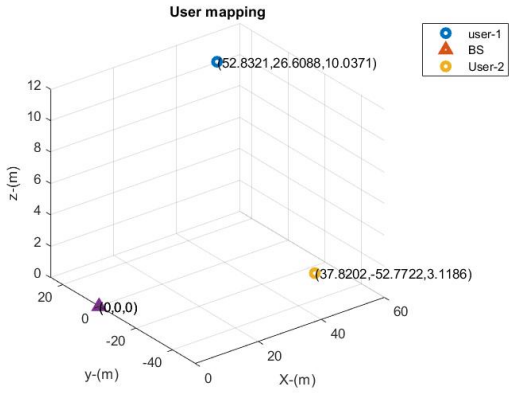

Figure 3.1: User distribution in a cell

3.2. Performance Metrics

Performance evaluation of a communication system is done using common metrics like EVM, BER, and SNR [74]. For the developed system, we use two main performance indicators: EVM and BER along with the constellation diagram. The receive constellation diagram of the equalized symbols gives a qualitative measure of signal reception. Whereas, EVM and BER offer a quantitative assessment of the signal received at the UE. BER provides the number of erroneous bits present. Due to its simplicity in evaluation, it is a widely used performance metric amongst engineers and scientists. It is calculated as the ratio of the number of error bits N_{err} to the total number of received bits N_{bits}. BER is a direct consequence of channel noise [74]. In our simulations, in most of the cases, the BER for the users remains zero. The reason being, the noise level is low, and an efficient channel coding is able to decode the data bits correctly. However, in cases when interference power is dominating, we see that the BER is a non-zero value.

$$BER = \frac{N_{err}}{N_{bits}} \tag{3.1}$$

Lately, the use of EVM as a performance indicator for 5G massive MIMO system has been highlighted in many research works [75], [76], [77]. For digital communication systems, it is an important parameter that quantifies the modulation linearity of the transmitted signal. It helps to identify the phase and amplitude deviations experienced by the transmitted signal as it traverses through the channel [78]. To calculate EVM, we can use the equation 3.2. The EVM limits for different modulation schemes for 5G NR signals set by 3GPP are given in Table 3.2.

$$EVM_{RMS} = \sqrt{\frac{\frac{1}{N}\sum_{n=1}^{N}\left|s_r(n) - s_t(n)\right|^2}{\frac{1}{N}\sum_{n=1}^{N}\left|s_t(n)\right|^2}} \tag{3.2}$$

Here, N is the total number of symbols, $s_r(n)$ is the normalized received symbols after equalization and $s_t(n)$ is the ideal value of the n^{th} symbol [79]. This can be easily understood from Figure 3.2. The black dots represent the ideal symbols in this 16-QAM constellation diagram, while the red dot is the received symbol. The average amplitude of the error vector P_{error} normalized to peak signal amplitude gives the EVM. EVM is frequently used to characterize signals that use the broadband system for higher data rates due to the potential mixing of in-band frequency components. Since EVM values are reported as normalized values, it enables us to use for direct comparison between different modulation schemes[80]. When we consider a MU-MIMO system, precoding techniques such as zero-forcing(ZF), Minimum Mean Square Error(MMSE), etc. becomes inevitable for a reliable data transmission [81]. Such precoding techniques are used to suppress the interference between the users, provided that perfect CSI is available at the BS. However, when the CSI is obtained after channel sounding, it will contain errors that might occur due to local oscillator, phase noise, quantization errors, etc. [82]. Hence, the interference caused due to the inaccuracy in real-time CSI is not suppressed by the precoding algorithms, and this raises concerns about the signal to interference plus noise ratio as a performance indicator in MU-MIMO systems. Because the interference value caused by inaccurate CSI is unknown, determining the SINR value in real-time is not feasible. [79]. A comprehensive metric that can cover the inaccuracies due to CSI, as well as interference between the users, is EVM. Moreover, compared to BER, it can be measured at an earlier stage, i.e. before demodulation and demapping of the received signal.

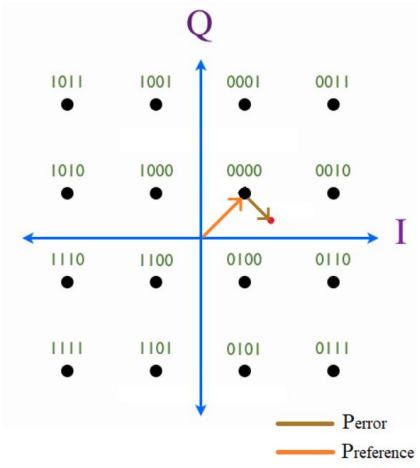

Figure 3.2: Ideal 16-QAM constellation diagram [7]

PDSCH Modulation	Limit(%)
QPSK	18.50
16-QAM	13.50
64-QAM	9.00
256-QAM	4.50

Table 3.2: EVM PDSCH Limits from 3GPP TS 38.104 [9]

3.3. Regular Planar Array At The Base Station

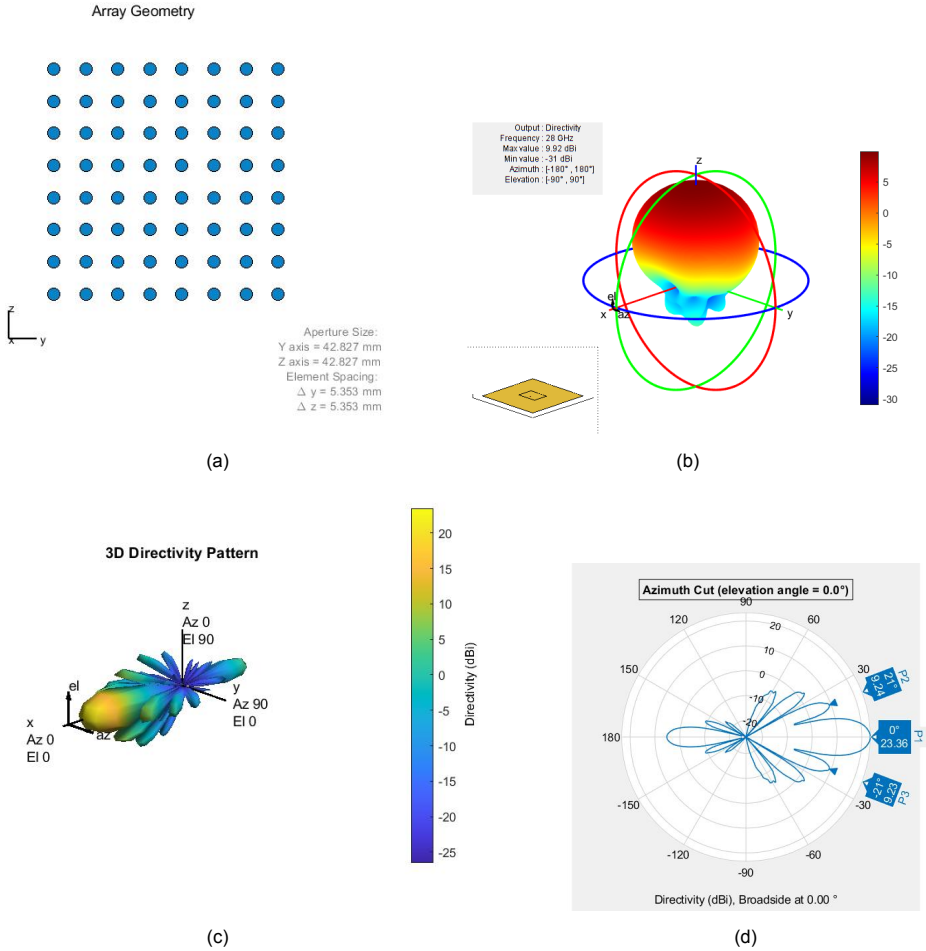

Figure 3.3: BS Antenna array design,(a)Array Layout,(b)Element patch radiation pattern,(c)3-D radiation pattern of the array,(d)Azimuth Cut

Currently, 5G base stations employ the regular periodic phased arrays. This topology is motivated by the fact that it is easy to be designed and manufactured, as well as it is cost-efficient. For this case study, we consider an 8x8 uniform rectangular array(URA) of patch elements as shown in Figure 3.3a. The array is placed in the Y-Z plane, and it is carefully designed in such a way that every element is separated by a distance of $\lambda/2$ in order to avoid grating lobes. The single element of the array is a patch antenna designed for the center frequency 28GHz. The design specifications of the patch antenna are given in Table 3.3 and Figure 3.3b represents its radiation pattern. The 3-D directivity pattern of the array is given by Figure 3.3c and the azimuth-cut is displayed in Figure 3.3d. The maximum directivity obtained while using this array is 23.36dB at the broadside direction, and the sidelobe directivity is 9.63dB. A higher back lobe is visible due to the limited length of the ground plane of the patch element. The azimuth half-power beamwidth is measured to be approximately 13°. In the following sections, we investigate the use of this array at the BS for different case studies as mentioned earlier.

Parameters	Value(mm)
Length	5.1
Width	6.7
Ground Plane Length	21.4
Ground Plane Width	21.4
Height	0.107

Table 3.3: Patch antenna element parameters

3.3.1. Study Of User Range

In this section, we study the impact of how changing the range of the users affects the performance of the users in terms of EVM. Let us consider that User-1 is at a fixed position, i.e. situated at 50 meters from the BS. Table 3.4 summarizes the positions of the BS and the users in the system. The azimuth and elevation of users are defined randomly. We transmit two data streams from the BS to the corresponding UE and the performance is evaluated at the user end. Now, we conduct Monte Carlo simulations for different ranges of User-2 and measure the EVM values for each user. The relation between the range and EVM of users is depicted in Figure 3.4. In order to observe the data trend, a curve fit of the EVM results are also plotted. It can be seen that the EVM of User-1 is almost a constant, and it remains to be within 2 and 3.5%. For User-2, we see a higher fluctuation in EVM between 0.5% and 5%. From the curve fit graph for User-2, we see a slight increase in the EVM as the range increases. In general, it is hard to predict a trend for User-2 EVM values. The curve possibly verifies that the EVM values are independent of the range. We see random fluctuations in the EVM values, which could be the influence of rich scattering and multipath effects from the channel.

Parameter	BS	User-1	User-2
Range(m)	0	50	50 to 200
Azimuth(deg)	0	26.732	-54.372
Elevation(deg)	0	9.639	2.756

Table 3.4: BS and User position

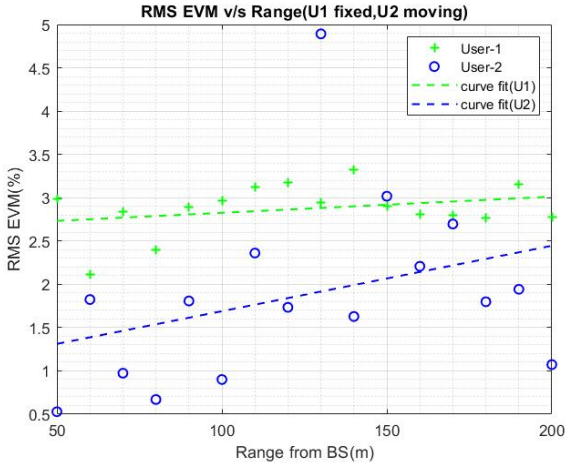

Figure 3.4: EVM v/s Range

3.3.2. Study of User Position In Azimuth

The following case study highlights the effect of changing the azimuth separation of the users on EVM and BER. For this purpose, we keep all the other position parameters as constant and vary the azimuth of User-2 from -60 to 60° in steps of 6°. Table 3.5 gives the position parameters of the users and BS. From Figure 3.5, it is evident that the azimuth separation between users plays a major role in the EVM values. As User-2 moves closer in azimuth towards User-1 i.e. around -40°, we see a steep rise in EVM for both users. User-2 reports the highest EVM of 37.746% when it is around -40° in azimuth. Whereas, User-2 records a maximum of 24.021%. Both values are way above the permissible limits specified by 3GPP [Table3.2] shown by the red line. In order to fall within the interference limit, User-2 should be at an azimuth angle less than -50.67° and greater than -23.31°. From the graph, we can see that as users get more separated in azimuth, there is a decrease in the EVM values. The reason for such trends in the graph is due to the interference experienced by the users when they are closely separated in azimuth. In this case, both the users are highly correlated, and we see a decrease in the performance. Hence, we can say that from -50 to -35°, EVM values are dominated by the interference effect. A closer look at the precoded transmit patterns of the BS towards each user can help to understand graphs.

Parameter	BS	User-1	User-2
Range(m)	0	50	110
Azimuth(deg)	0	-40	-60 to 60
Elevation(deg)	0	9.639	2.756

Table 3.5: BS and User position

Case-1

Let us consider the scenario when User-2 is at azimuth angle -42° while User-1 is fixed at -40°. The precoding weights obtained from the channel are applied to User-1 and User-2, and their directivity patterns are shown in Figure 3.6. An interesting point to be noted is that for both the users, the main lobe is not exactly directed towards the user and hence, the directivity values experienced by the users are much lower(14.36dB for User-1 and 1.725dB for User-2). This is due to the fact that when a generalized channel inversion technique is applied to suppress the interference, the main lobe gets shifted away from the exact user location when both the users are closer to each other in an attempt to cancel the interference towards the other user. Apart from that, we can notice high side lobes, which contribute to the interference faced by the users. The interference

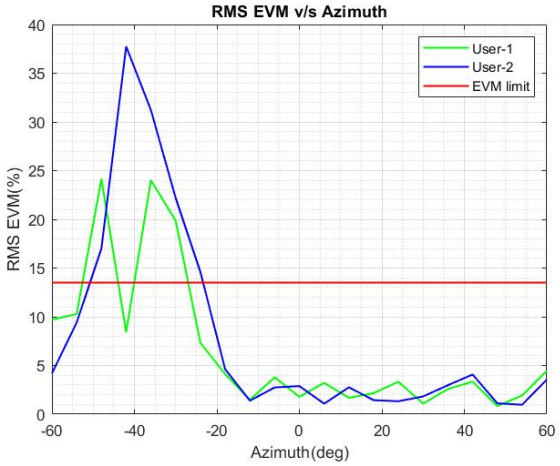

Figure 3.5: EVM v/s Azimuth angle

is measured as the difference in the power directed to the main lobe and power directed to its side lobes. Hence, the interference faced by User-1 is -25.03dB(14.36-(-10.67)) while User-2 faces higher interference of about 2.598dB(1.725-4.323). This explains why User-2 has higher EVM than User-1. The corresponding effect is also seen in the constellation diagram shown in Figure 3.7. The EVM, BER values are summarized in Table 3.6. We can see that while User-1 is able to decode the bits correctly, User-2 suffers from noise, resulting in errors while decoding.

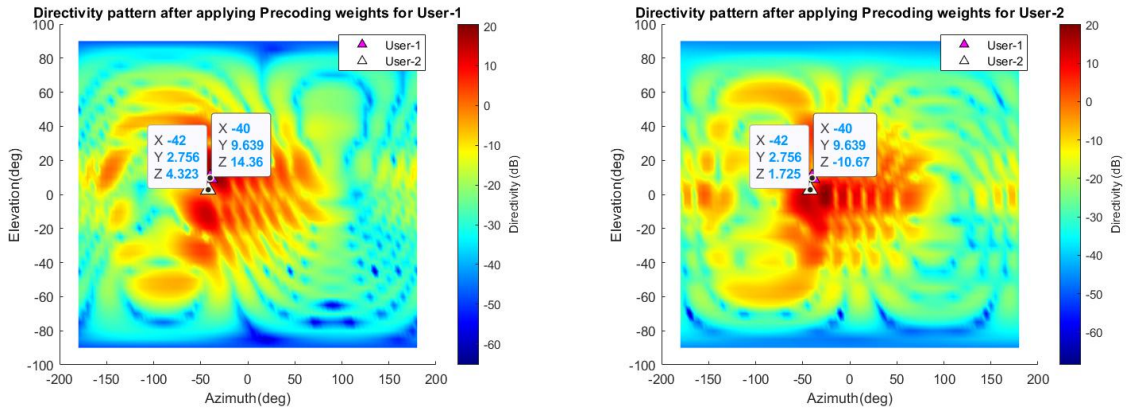

Figure 3.6: Directivity pattern after applying precoding weights when User-2 is at an azimuth angle -42° (a)User-1(b)User-2

User	EVM	BER
User-1	8.428%	0.000 • No. of bits=3114 • No. of errors=0
User-2	37.746%	0.019 • No. of bits=3114 • No. of errors=62

Table 3.6: EVM and BER values when User-2 is at -42°(Azimuth)

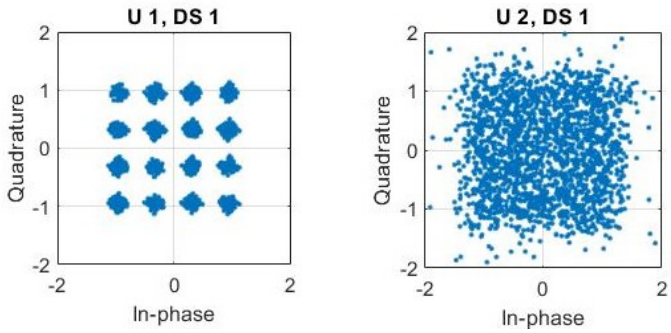

(a) (b)

Figure 3.7: Constellation diagram (a)User-1(b)User-2

Case-2

Now, let us explore the case when User-2 is at azimuth angle 48°. The directivity of the precoded patterns for both users is given in Figure 3.8. We can observe that compared to the previous case, the directivity values towards the users have improved drastically, with User-1 having 21.4dB and User-2 with 19.65dB. Apart from that, there is a considerable reduction in the interference experienced by both the users, i.e. -56.21dB and -37.56dB for User-1 and 2 respectively. The constellation diagram is given in Figure 3.9 and EVM, BER values are specified in Table 3.7. We can see that the obtained constellation diagram is of high quality. As a result, the EVM and BER values have also been reduced.

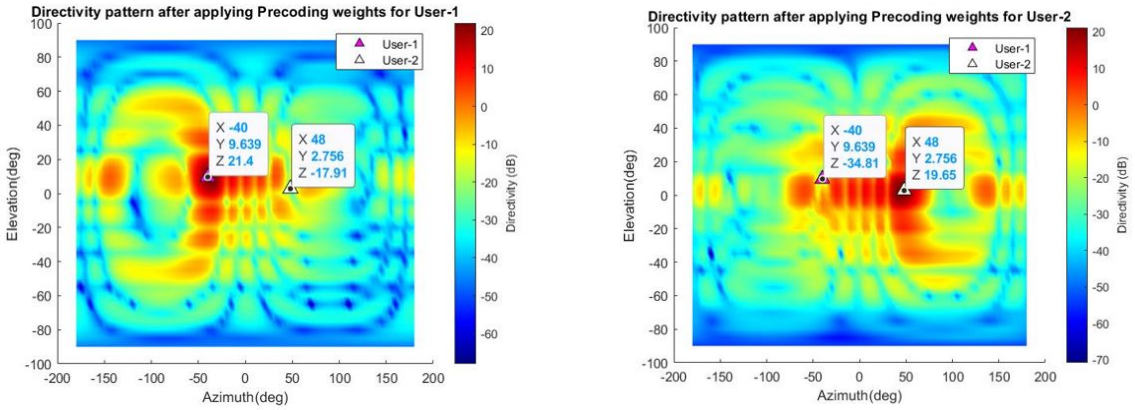

(a) (b)

Figure 3.8: Directivity pattern after applying precoding weights when User-2 is at an azimuth angle 48° (a)User-1(b)User-2

User	EVM	BER
User-1	0.827%	0.000 • No. of bits=3114 • No. of errors=0
User-2	1.108%	0.000 • No. of bits=3114 • No. of errors=0

Table 3.7: EVM and BER values when User-2 is at 48°(Azimuth)

Hence, we can conclude that when users are spatially separated well enough in azimuth, the

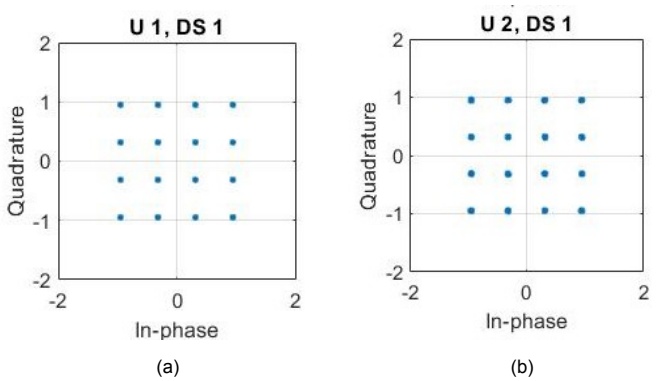

(a) (b)

Figure 3.9: Constellation diagram (a)User-1(b)User-2

performance of the users is improved. The angular separation is influenced by the beamwidth of the assigned beams. The minimum angular separation between the two beams should be at least the value of beamwidth in order to have low interference. In some research work like [83], the author discusses an interference aware approach where users have angular separation greater than the half-power beamwidth of the regular antenna array.

3.3.3. Study of User Position In Elevation

In this case study, we are going to investigate the influence of changing elevation of the users and evaluate the performance in terms of EVM and BER. Let us assume that User-1 is fixed at the range 50 meters and User-2 at 110 meters from the BS. Both the users are closely separated in azimuth and elevation. The user and base station positions are provided in Table 3.8. We perform Monte Carlo simulations for the system by varying elevation angles of User-2 from -15 to 15° in steps of 3°. The graph in Figure 3.10 depicts the EVM versus elevation angle for both User-1 and User-2. We can see from the figure that there is an increasing trend in EVM when the User-2 is approaching the elevation angle of User-1, after which the EVM curve descends. A similar observation was made for the azimuth angle case study. The result is as expected, since the downlink interference between the User-1 and User-2 beam increases when the users are closely separated in azimuth and elevation. It can be noted that for User-2 until 0°, we have permissible EVM values, after which the values are considerably larger than the upper limit specified by 3GPP which is shown by the red line. Apart from that, it can be seen that User-2 faces less interference from User-1 up to 2°, after which the EVM values of User-2 rise above User-1. This could be because the interference faced by User-2 due to User-1 is more than the interference faced by User-1 due to User-2. In the following part of this section, we will investigate the case when the EVM value is the highest and the lowest.

Parameter	BS	User-1	User-2
Range(m)	0	50	110
Azimuth(deg)	0	20	24
Elevation(deg)	0	9	-15 to 15

Table 3.8: BS and User position

Case-1

Let us consider the scenario when User-1 and User-2 have the lowest EVM, i.e. when User-2 is at an elevation angle -15°. Corresponding directivity plots after applying precoding weights to the transmit array pattern are shown in Figure 3.11. By looking at the Figure 3.11a and 3.11b, we can calculate the interference experienced by User-1 as -36.90dB and User-2 as -42.21dB. Table 3.9 provides the

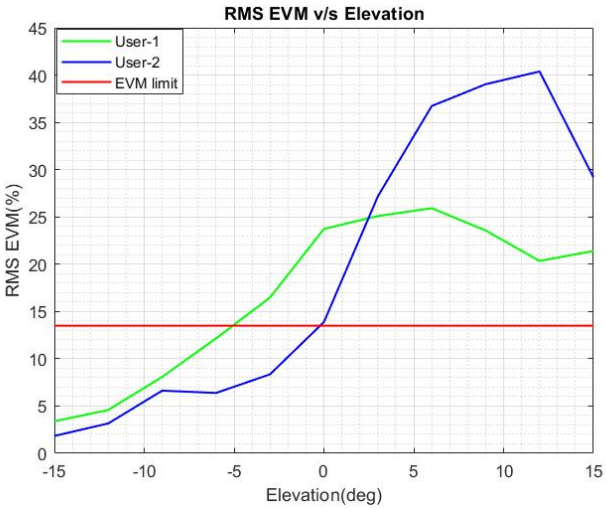

Figure 3.10: EVM v/s Elevation angle

evaluated performance metrics for both users. Both users are having low EVM values while BER is zero. This is further supported by a good quality constellation diagram of the received signal streams given in Figure 3.12. Hence, we can conclude that even though the users were closely separated in azimuth, by ensuring sufficient separation in elevation, we can control interference between them to a larger extent.

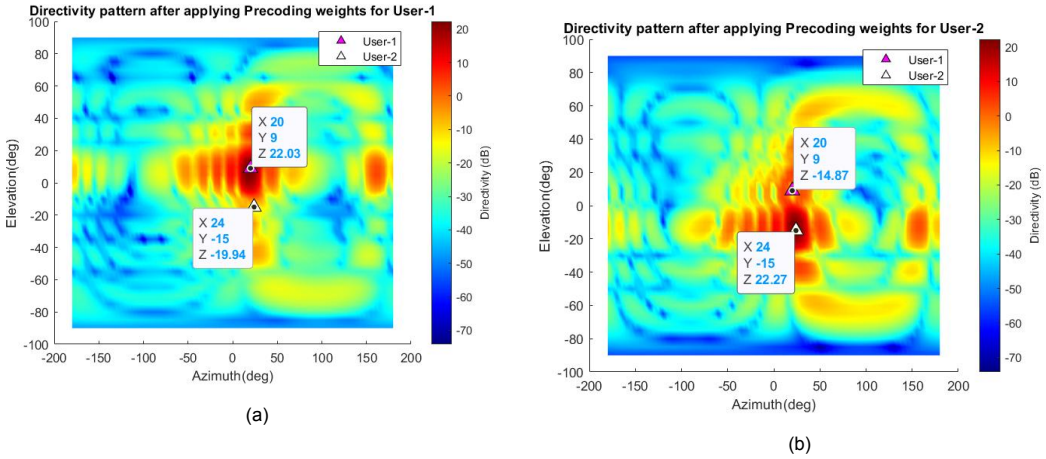

Figure 3.11: Directivity pattern after applying precoding weights when User-2 is at an elevation angle -15° (a)User-1(b)User-2

User	EVM	BER
User-1	3.383%	BER=0.000 • No. of bits=3114 • No. of errors=0
User-2	1.838%	BER=0.000 • No. of bits=3114 • No. of errors=0

Table 3.9: EVM and BER values when User-2 is at -15°(Elevation)

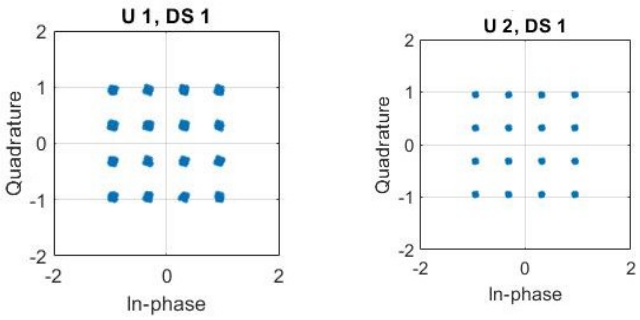

(a) (b)

Figure 3.12: Constellation diagram (a)User-1(b)User-2

Case-2

When User-2 is at an elevation angle of 12°, it experiences a maximum EVM of 40.379%. In order to get some physical insight, let us plot the directivity patterns of the precoded transmit array pattern. From Figure 3.13a and 3.13b, we can notice that the main lobe of the beam is directed away from both the users, which has lead to a decrease in directivity experienced in comparison to the previous case. In addition, the interference faced by both users is very high with User-2 having -2.51dB and User-1 with -6.834dB which is comparatively lower than User-2. This is because the users are highly correlated and in such cases, BD precoding fails to mitigate the inter-user interference, and it leads to reduction of SNR. This in turn results in worse user performance, which can be verified from the constellation diagram in Figure 3.14 and the BER, EVM values in Table 3.10. User-1 reports an EVM of 20.314% while User-2 EVM is about twice that of User-1. From Figure 3.14a, we can observe that the received symbols cloud around the idealized symbol points due to the influence of noise. However, the received symbols fall within the decision boundaries due to which it is able to decode the bits without error. Whereas, the constellation for User-2 in Figure 3.14b shows that the received symbols are spread and also overlap with each other, which makes it hard for the decoder to recover the data bits. Hence, we have a BER of 0.07 for User-2. A point to be noted in this case is that the reported results would improve in situations where the users are well separated in the azimuth direction.

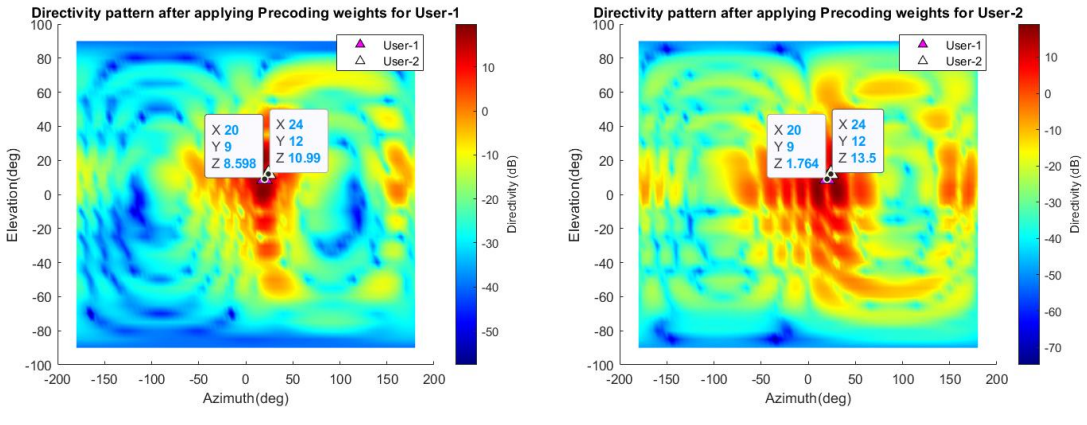

(a) (b)

Figure 3.13: Directivity pattern after applying precoding weights when User-2 is at an elevation angle 12° (a)User-1(b)User-2

User	EVM	BER
User-1	20.314%	BER=0.000 • No. of bits=3114 • No. of errors=0
User-2	40.379%	BER=0.070 • No. of bits=3114 • No. of errors=219

Table 3.10: EVM and BER values when User-2 is at 12°(Elevation)

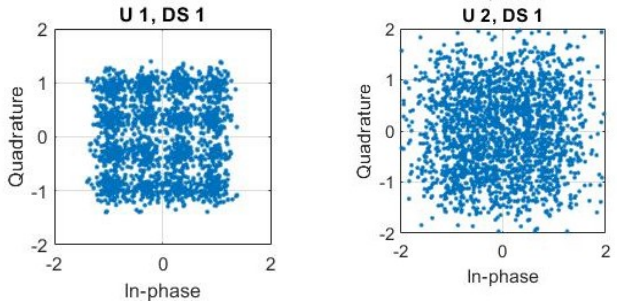

(a) (b)

Figure 3.14: Constellation diagram (a)User-1(b)User-2

3.3.4. Increasing The Number Of Transmit Elements

In this case study, we investigate the effect of increasing the number of elements in the BS antenna array on the performance of users in the system. We consider a 16x16 uniform rectangular array at the BS, i.e. we have M=256 patch elements as shown in Figure 3.15a. The 3-D radiation pattern for the array is given in Figure 3.15b and the azimuth cut is displayed in Figure 3.15c. We can observe that increasing the array size has resulted in increase in the directivity of the mainlobe to about 27.4 dB. Another important fact to take into account is the reduction in beamwidth. For this case, the half-power beamwidth in azimuth is about 5.52°. A reduction in beamwidth can in turn reduce the interference between the users when they are closely separated. Hence, the performance of the users will be determined by the correct application of precoding weights to reduce the interference effects.

In this section, we will evaluate the performance of users when 16x16 URA is used at the BS and compare it with the results of Section 3.3.1 to 3.3.3. To begin with, we perform the case study when the range of the User-2 is changed progressively. We will be exploring if the change in the array size would make an impact on the EVM values. Same user and BS position is considered as mentioned in Table 3.4. The EVM values corresponding to both the arrays are plotted against the varying range of User-2 in Figure 3.16. From the curve fit graph of M=256, we can notice that the EVM values are almost constant as User-2 moves away from User-1. When we compare the EVM values between the M=64 and M=256 antenna array, we see that in most cases, EVM values attained by the larger array is less. This could be because the use of high gain arrays results in more received power to the user and hence we have less EVM. A similar observation is made in [84, Fig. 8a], where the author compares average received EVM as a function of array sizes for different channel models. However, this effect is mostly observed provided the antenna array is able to steer the beam exactly to the user location. Since we do not have a perfect channel, there can be the case when the main

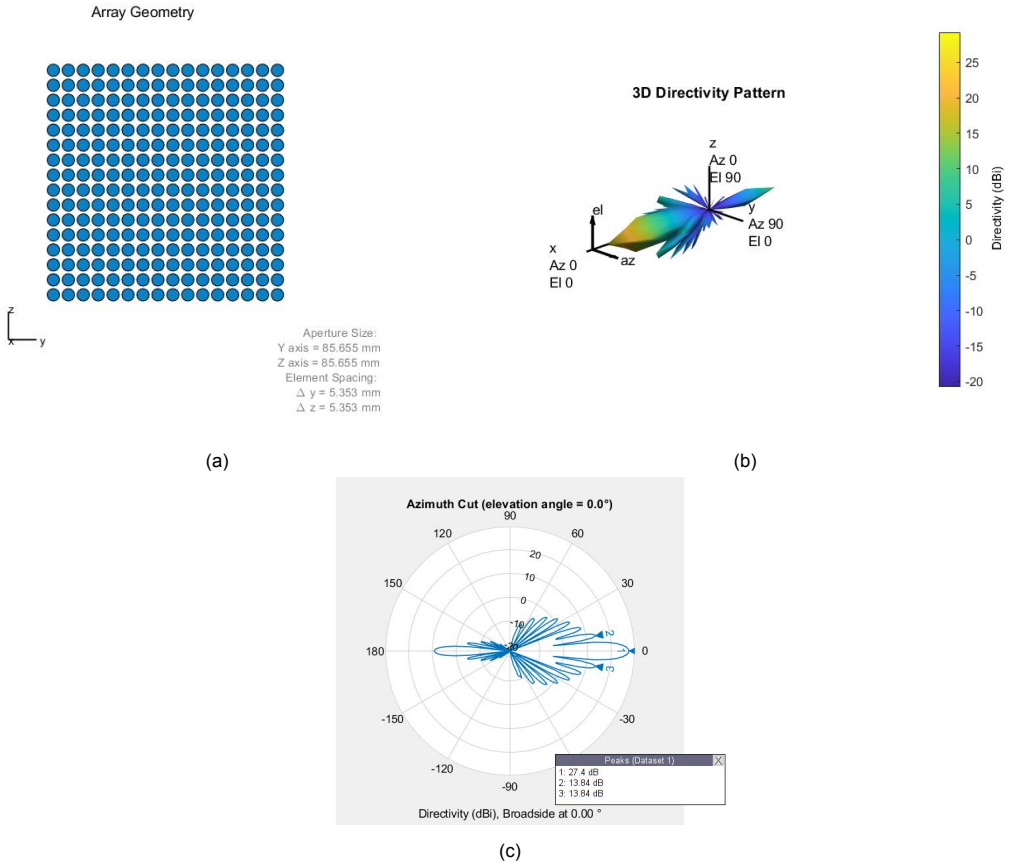

Figure 3.15: BS Antenna array design (a)Array Layout with M=256,(b)3-D radiation pattern of the array,(c)Azimuth cut

lobe of the beam is slightly shifted away from the user, which might result in higher EVM. Apart from that, we notice that EVM values are fluctuating rapidly, which might be due to the rich multipath nature of the channel.

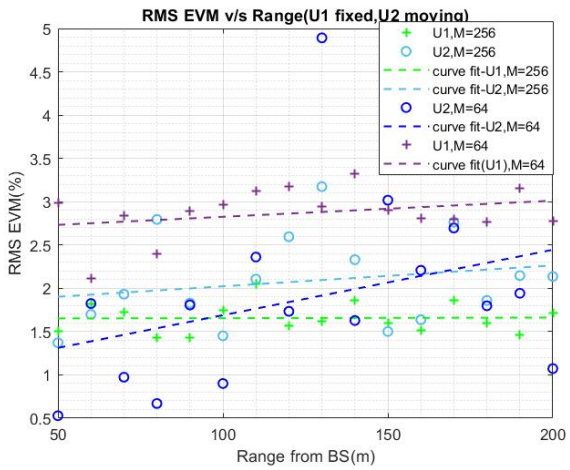

Figure 3.16: Comparison of EVM values for different array sizes for a varying range of User-2

Secondly, we conduct the scenario where the azimuth is varied for User-2. The user positions remain the same as that of Table 3.5. Figure 3.17 draws a comparison of the EVM values obtained for both the users for M=64 and M=256 elements at the BS. We can observe that there is a slight improvement of EVM for User-2 while for User-1, we see a considerable reduction in the EVM. At

around -42°, for User-1, there is a minimal decrease of EVM of about 2%. For User-1, there is a reduction of about 7% at the two peaks, which are at -36° and -48°. The red line shows the specified EVM limit. In order to fall within the permitted EVM limits, User-2 should be at an azimuth angle less than -50.14° and greater than -27.63 while using the larger array. However, for the 8x8 array, this range is less and User-2 should be at an azimuth angle greater than -23.09°. The reason for this behavior could be because of the narrow beams generated when the antenna array size is increased at the BS. This in turn facilitates less interference between users when they are closely separated. However, this effect is not prominent as User-2 moves away from User-1, i.e. at an azimuth angle greater than -20°. In this case, we do not see much difference between the M=64 and M=256 curves.

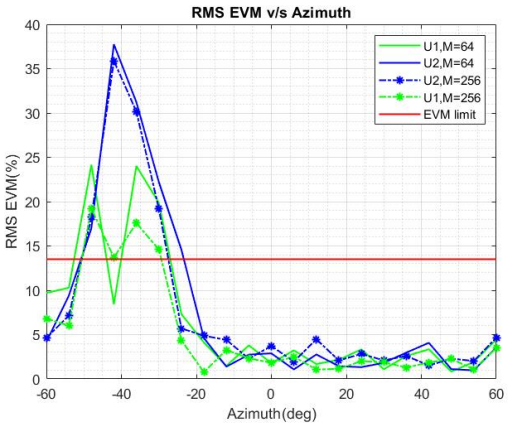

Figure 3.17: Comparison of EVM values for different array sizes for varying azimuth positions of User-2

In the next case, User-2 is varied in elevation as mentioned in Section 3.3.3 (Table 3.8). The EVM curves are evaluated for M=256 BS antenna array with respect to M=64 antenna array and the results are depicted in Figure 3.18. For both users, we see that EVM curves for M=256 almost follow the M=64 curve, with slight deviations at certain elevation angles. Additionally, both the arrays achieve similar closeness where User-2 should be at an elevation angle greater than 0° to be within the permissible EVM limits. Apart from that, we can see an improvement in EVM of about 8% for User-2 in comparison to the M=64 curve of User-2 at 9°. This is due to the fact that the interference experienced by User-2 for M=256 is about -9.35dB, which is lower than that faced by User-2 for M=64 that is -5.709dB. When we have a larger antenna array, the beamwidth of the beams reduces, which has helped to reduce the interference between the users.

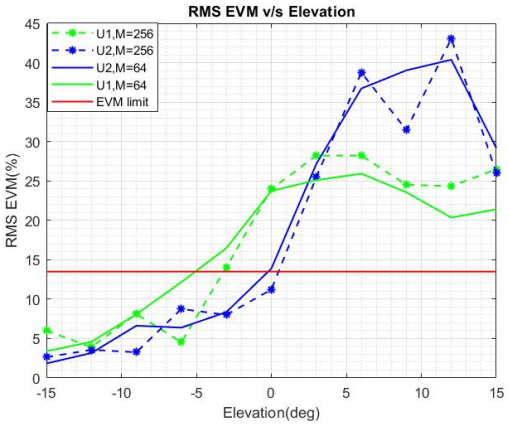

Figure 3.18: Comparison of EVM values for different array sizes for varying elevation positions of User-2

From Figure 3.17 and 3.18, we can conclude that only for the higher interference region, we are able to observe the improvement of EVM by using a large BS antenna array. Apart from that, the nature of graphs is not smooth. It has fluctuations that arises due to the effect of rich scattering channel with only multipath present. A point to be noted is that observations made are heavily dependent on the nature of the channel(LoS, NLoS). Hence, we might see a different behavior for the LoS case.

3.4. Irregular Planar Array At The Base Station

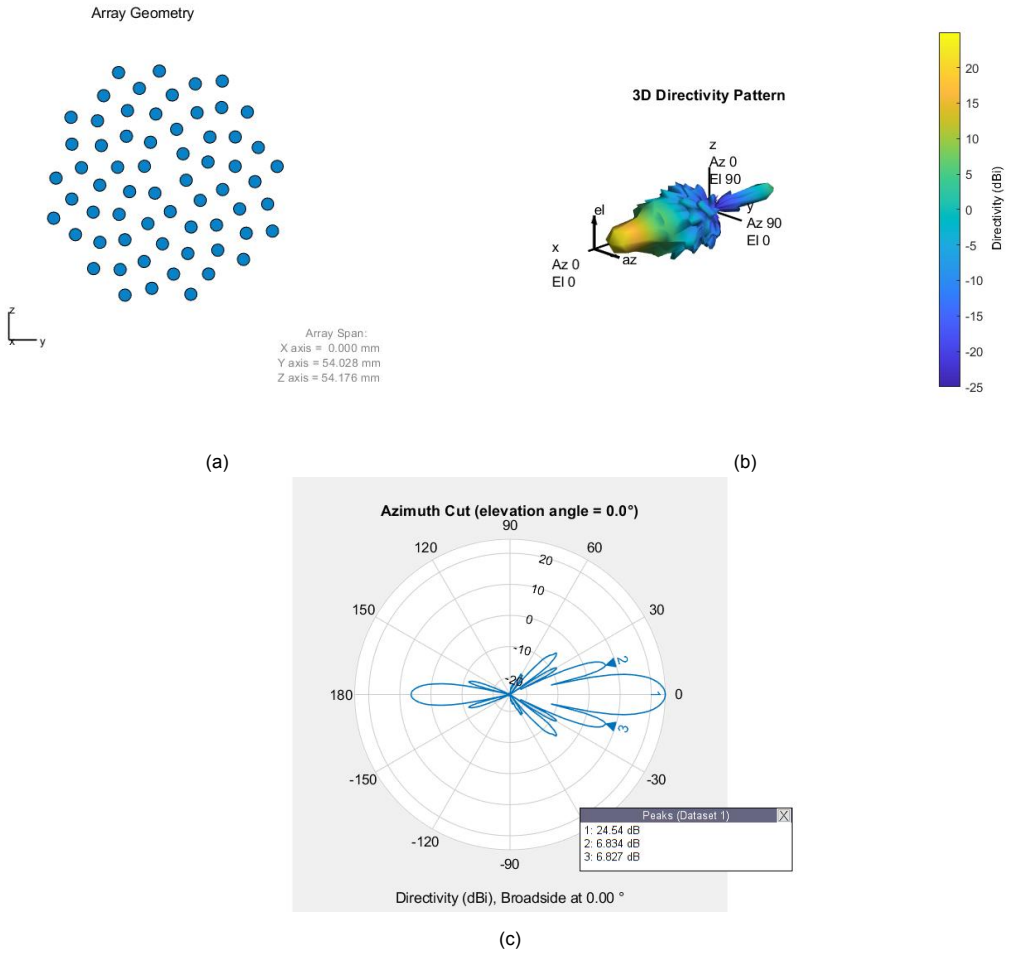

Figure 3.19: BS Antenna array design, (a)Array Layout, (b)3-D radiation pattern of the array, (C)Azimuth Cut

In this section, we investigate the use of an irregular aperiodic array as the BS antenna array, where the elements are organized in the Fermat lattice or sunflower structure. Compared to the periodic arrays, aperiodic arrays have several advantages. Firstly, the sidelobe levels are profoundly reduced without employing amplitude tapering. Another useful feature is the potential to use a fewer number of elements in one single aperture without compromising on the bandwidth [85]. Finally, aperiodic arrays decrease the effect of grating lobes due to incommensurable element spacing. The combined benefits of the sparsed aperiodic array are observed in the sunflower topology. The speciality of this configuration is that we do not have grating lobes and sidelobe levels are low. We will explore the use of such sunflower array configuration at the BS and evaluate the performance of the users. Further, we compare the results with that of the uniform rectangular array(regular array).

Let us consider the BS antenna array consisting of M=64 patch elements arranged according to the equations 3.3 and 3.4 where ρ_m is the distance from the centre of the spiral to the m^{th} element, s is the mean distance between the elements which is taken as 0.6λ. ϕ_m is the angular displacement between consecutive elements, and it is controlled by β. The value of β corresponds to that of the golden angle ($\beta = \frac{\sqrt{5}+1}{2}$) since it resembles the configuration of the sunflower seeds.

$$\rho_m = s\sqrt{\frac{m}{\pi}} \tag{3.3}$$

$$\phi_m = 2\pi m\beta \tag{3.4}$$

Figure 3.19a gives the layout of the BS antenna array and Figure 3.19b shows its 3-D radiation pattern. From Figure 3.19b, we can observe that the pattern has a single narrow main lobe and reduced sidelobe levels. The maximum directivity obtained with the array is 24.54dB, and the first sidelobe directivity is about 6.8dB. The half-power beamwidth is calculated to be around 10.9°.

3.4.1. Study Of User Range

With the irregular array, we perform the simulation scenario where the range of User-2 is varied, and the performance evaluation is conducted for both users in terms of EVM and BER. The same position parameters are used as mentioned in Section 3.3.1, Table 3.4. The EVM results are plotted against the range for both the users in Figure 3.20. It can be seen from the curve fit plots that the EVM values are almost a constant for both the users. EVM values for the User-1 range between 1.65% to 3.05%. Similarly, for User-2 it varies between 1.65% to 3.3%. As mentioned earlier, these fluctuations arise due to the nature of a rich scattering channel. The average EVM experienced by User-1 for the irregular array is about 2.278% while by using the regular array we observe a marginally higher EVM of about 2.872%. However, for User-2, while using the irregular array, the average EVM experienced is about 2.468% which is slightly higher compared to 1.878% when the regular array is used. Hence, we do not see much impact of using the irregular array topology at the BS for this case study. A point to be noted is that these results are completely dependent on the type of channel used. We might not observe the same results for other channel models.

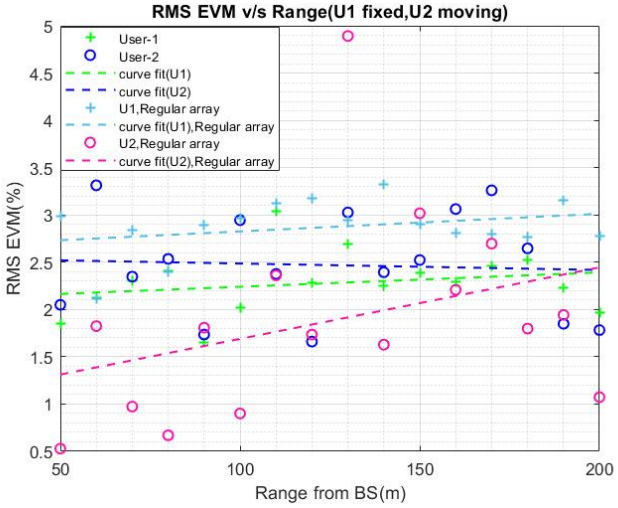

Figure 3.20: EVM v/s Range

3.4.2. Study Of User Position In Azimuth

In this case study, we are going to make a comparative analysis with the regular array and the irregular array while the azimuth of User-2 is varied from -60 to 60°. The user and BS locations

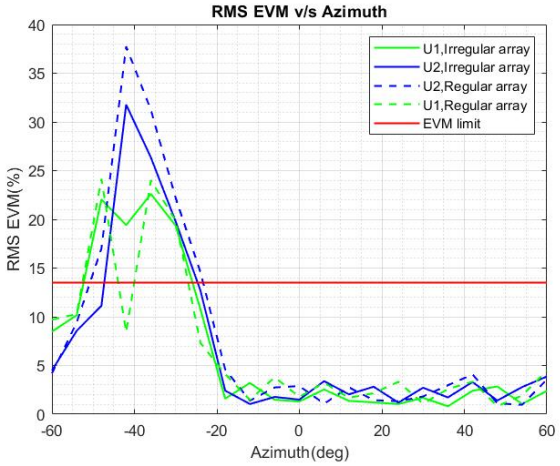

Figure 3.21: EVM v/s Azimuth

are summarized in Section 3.3.2, Table 3.5. Figure 3.21 draws the comparison between the EVM values obtained while using irregular and the regular array for the mentioned case. We also plot the permissible EVM limit (red line) specified by 3GPP for 16-QAM modulation, as given in Table 3.2. From the figure, we observe that the maximum EVM reported by User-2 while using the irregular array is about 31.77%, which is about 6% less than that reported while using the regular array. However, for User-1, we might see the opposite effect at -42° alone. Let us have a closer look at the precoded patterns for the irregular array given in Figure 3.22. The interference faced by User-1 is about -22.76 dB and for User-2 it is -0.145 dB. While using the regular array, we find that the interference faced by User-2 is 2.598 dB which is higher in comparison to the value obtained by using the irregular array. This is due to the lower sidelobe level for the irregular array. But for User-1, we see that the interference faced while using the regular array is less, i.e. -25.03dB, and EVM value is sharply reduced to 9%. The exact reason for this behaviour is not known. It could be due to the random placement of scatterers in the channel. Figure 3.23 shows the constellation diagram obtained for both the users while using the irregular array. User-2 shows a poor quality with noise dominated constellation. Whereas, for User-1, we are still able to distinguish the 16 distinct QAM symbols. Hence, we can see that the BER is 0 for User-1 while for User-2 it is 0.009 from Table 3.11. In order to fall within the specified EVM limits (13.5%), User-2 should be at an azimuth angle less than -47.27° or greater than -24.71° while using the irregular array. Whereas, for the regular array, User-2 should be at an azimuth angle less than -50.92° or greater than -23.42°. Hence, User-2 can be more closely separated from User-1 when the mentioned irregular array is used.

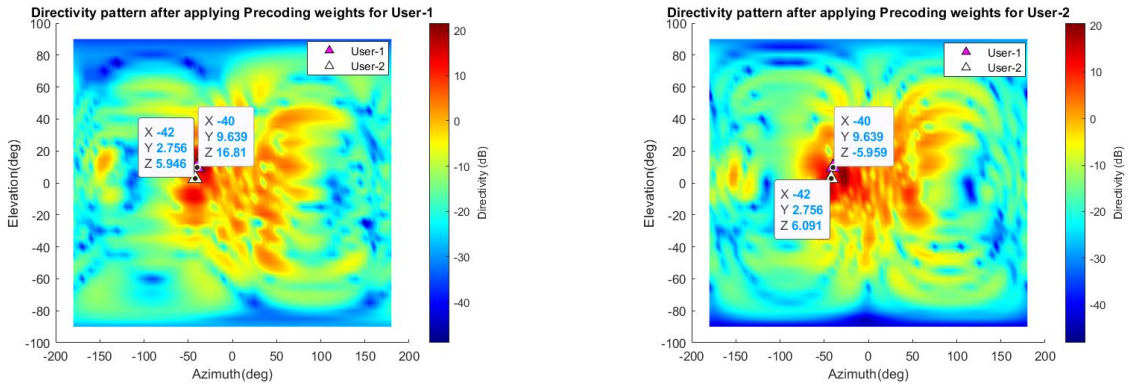

(a) (b)

Figure 3.22: Directivity pattern after applying precoding weights when User-2 is at an azimuth angle -42° (a)User-1(b)User-2

User	EVM	BER
User-1	19.408%	BER=0.000 • No. of bits=3114 • No. of errors=0
User-2	31.772%	BER=0.009 • No. of bits=3114 • No. of errors=30

Table 3.11: EVM and BER values

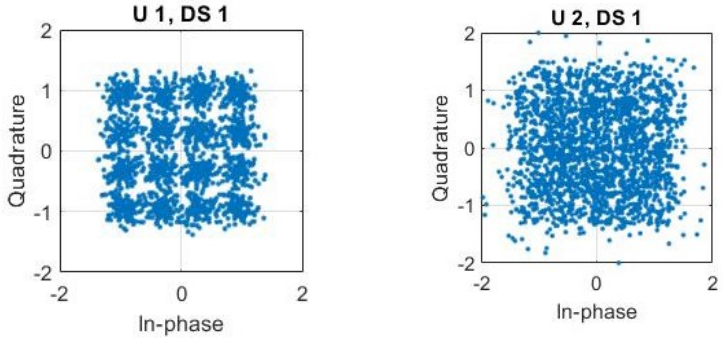

(a) (b)

Figure 3.23: Constellation diagram(a)User-1(b)User-2

3.4.3. Study Of User Position In Elevation

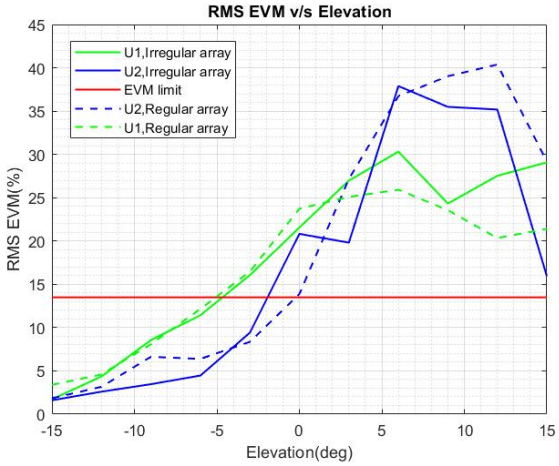

Figure 3.24: EVM v/s Elevation

In this section, the simulation scenario is performed by varying the elevation angle of User-2, similar to Section 3.3.3. Table 3.8 in Section 3.3.3 gives the overview of the BS and user locations. Like the previous case, we compare the performance of users while using the irregular and regular array topology at the BS. From Figure 3.24, we see that the EVM values of both the arrays are almost the same for two users. At 12°, there is an improvement in EVM of about 5% for User-2 while an irregular array is employed. From the transmit precoded pattern plotted in Figure 3.25, there are two beams directed towards the users. This can lead to very high inter-user interference since users

are close by. The interference faced by User-1 and User-2 is about -3.84 dB. When we compare these values to that of the regular array in Section 3.3.3, the interference faced by User-2 is higher, and it is about -2.51 dB while for User-1, it is about -6.83 dB which is lower compared to the irregular array. Figure 3.26 gives the constellation diagram obtained for this case. We see that both User-1 and User-2 have degraded signal quality. Table 3.12 gives the summary of the EVM and BER values reported by the users for this case. Additionally, to be within the specified EVM limits, User-2 should be at an elevation less than 13.5° while using the irregular array. Whereas, while using the regular array, User-2 should be at an angle less than 13.8°. Therefore, there is only a slight difference in these angles between both types of arrays such that they fall within the specified EVM limits.

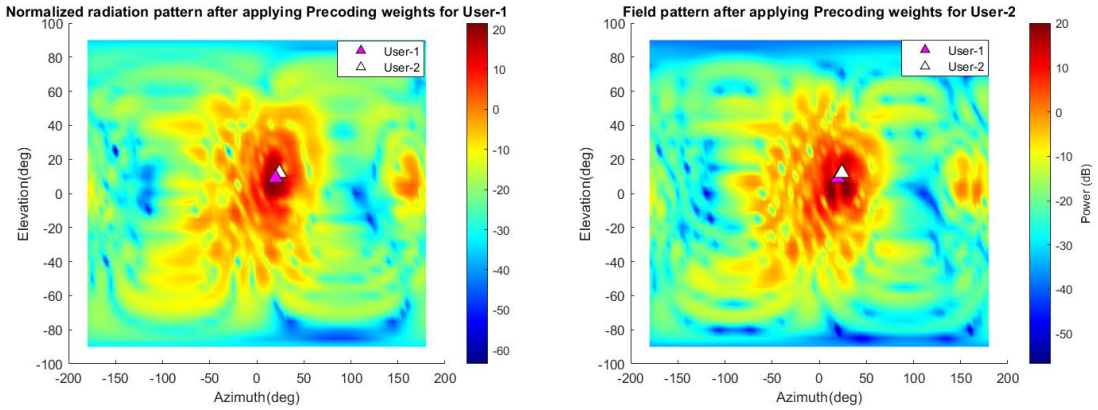

(a) (b)

Figure 3.25: Directivity pattern after applying precoding weights when User-2 is at an elevation angle 12° (a)User-1(b)User-2

User	EVM	BER
User-1	32.570%	BER=0.014 • No. of bits=3114 • No. of errors=44
User-2	38.864%	BER=0.023 • No. of bits=3114 • No. of errors=74

Table 3.12: EVM and BER values when User-2 is at 12°(Elevation)

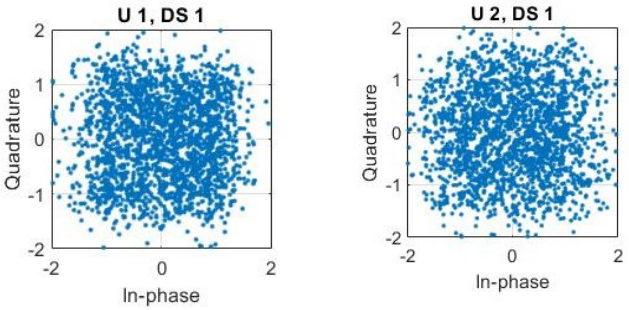

(a) (b)

Figure 3.26: Constellation diagram (a)User-1(b)User-2

3.4.4. Increasing The Number Of Transmit Elements

In this section, we are going to increase the number of transmit elements to about four times (M=256) and check the impact on user performance by repeating the case studies mentioned in Sections 3.3.1 to 3.3.3. Figure 3.27a gives the aperiodic array layout. The radiation pattern and azimuth cut is shown in Figure 3.27b and 3.27c respectively. When we increase the array size, we obtain a pencil beam with a directivity of about 28.03dB. The first sidelobe directivity has now increased to 10.07dB. The half-power beamwidth is measured to be about 5.4°.

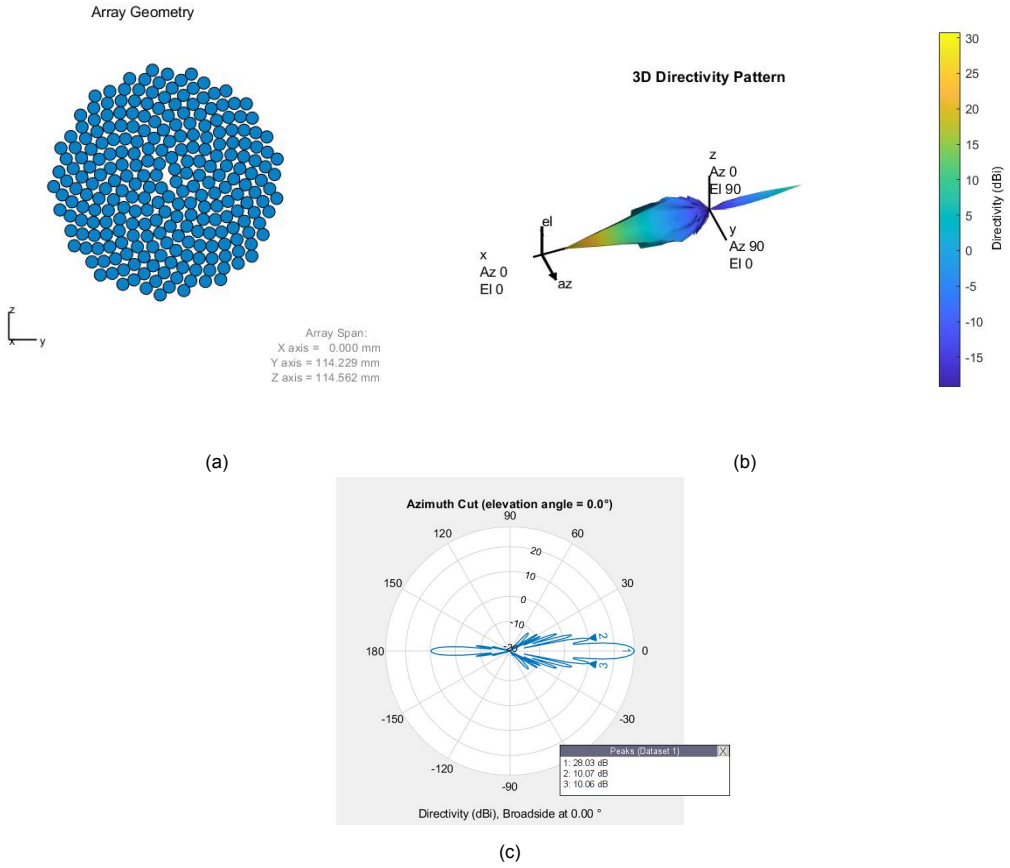

Figure 3.27: BS Antenna array design, (a)Array Layout, (b)3-D radiation pattern of the array, (C)Azimuth Cut

Firstly, we will vary the range of User-2, keeping User-1 fixed. The same simulation scenario in Section 3.3.1 is performed, and the result is shown in Figure 3.28. From the curve plots, we can see that there is slight decrease of EVM values when we use the larger array. This improvement in EVM could be due to the increase in array gain while utilizing a larger array. For User-1, the EVM reported is about 1.9% for M=256 and remains constant while User-2 is moved away from User-1. Whereas, for the smaller array (M=64), the EVM reported is about 2.2%. On average, User-2 experiences an EVM of 1.739% when 256 element array is used at the BS and about 2.5% when 64 element array is used. The results obtained for the irregular array is very similar, and hence we have not shown in the Figure 3.28.

In the next case, we vary the azimuth of User-2 from -60 to 60°, keeping User-1 at -40°. The same user and BS position are used as simulation parameters as mentioned in Section 3.3.2, Table 3.5. Figure 3.29 gives the comparison of EVM values obtained for both regular and irregular array consisting of M=256 elements. It can be observed that the EVM trends are almost similar for both

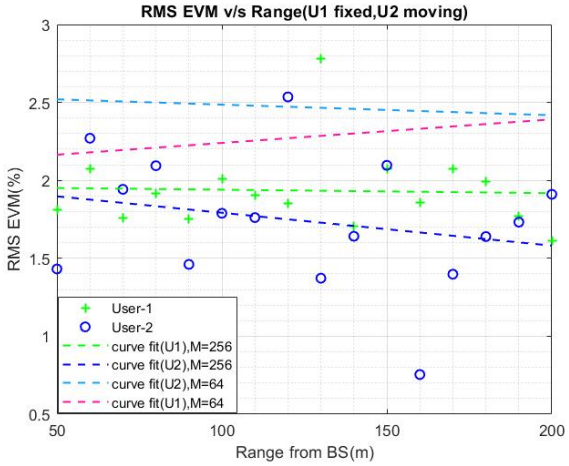

Figure 3.28: EVM v/s Range

curves. However, with the regular array, we can see a slight reduction in the EVM values at the peaks. When User-2 is at -42°, we find that it has a maximum EVM of about 41.3679% for the irregular array. Whereas, for the regular array there is about 6% reduction in EVM and the reported value is 35.87%. As a consequence, the BER is also higher, i.e. 0.093 for the irregular array and 0.066 for the regular array. The red line in the graph denotes the specified EVM limits for 16-QAM modulation. We can notice that for the irregular array, the EVM limit is achieved when User-2 is at an azimuth angle less than -49.71° and greater than -26.98°. This is almost the same for the regular array, with User-2 azimuth angle should be less than -50.84° and greater than -27.49°. Hence, we can see that both the arrays perform similarly to stay within the EVM limits. Let us have a closer look at the precoding patterns shown in Figure 3.30 for the irregular array when User-2 is at -42°. The interference faced by User-1 is about -25.135dB, and for User-2 it is -5.87dB. When comparing the interference values faced by User-2 while using the regular array, it is 0.07dB, which is higher. However, the EVM for this case is still lower in comparison to the irregular array. There could be other contributions to the noise other than interference in this situation, which is not explicitly known to us. From the constellation diagram obtained at the receiver in Figure 3.31, we can confirm that both the signals suffer from high noise levels. The EVM and BER values in Table 3.13 further supports this observation.

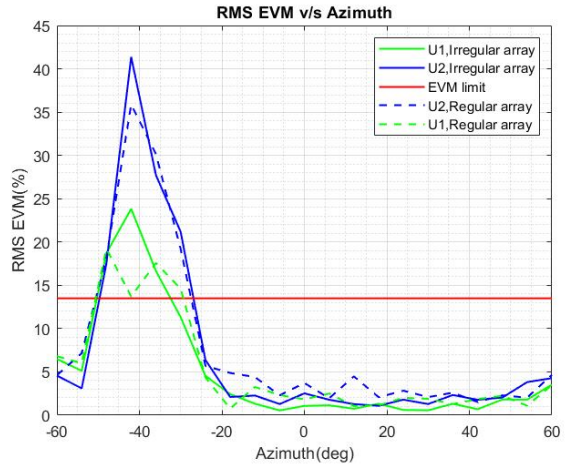

Figure 3.29: EVM v/s Azimuth

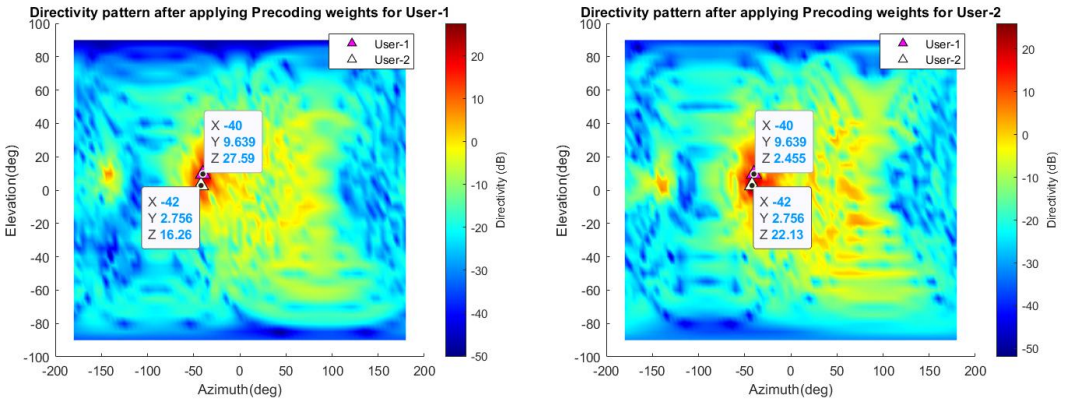

(a) (b)

Figure 3.30: Directivity pattern after applying precoding weights when User-2 is at an azimuth angle -42° (a)User-1(b)User-2

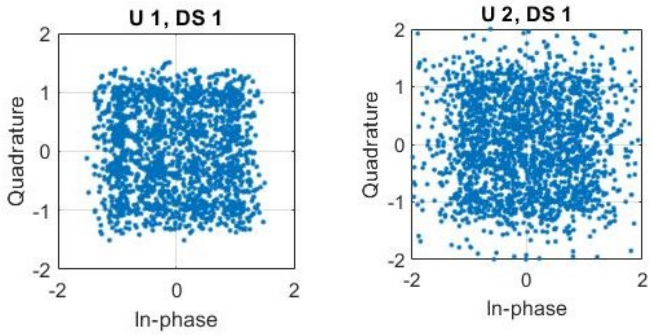

(a) (b)

Figure 3.31: Constellation diagram (a)User-1(b)User-2

User	EVM	BER
User-1	23.829%	BER=0.000 • No. of bits=3114 • No. of errors=0
User-2	41.367%	BER=0.093 • No. of bits=3114 • No. of errors=290

Table 3.13: EVM and BER values when User-2 is at -42°(Azimuth)

Finally, we analyze the last case study, which is changing the elevation of User-2. A similar approach is followed as mentioned in Section 3.3.3 and Table 3.8 gives the user and BS positions. Figure 3.32 gives the comparison of EVM values obtained for this simulation for both the regular and irregular array. For User-2, both the arrays almost follow the same curve with a slight difference in magnitude. Whereas, for User-1, the peak EVM value while using the regular array is 8% less than that of the irregular array. However, for User-2, we see a reduction in the peak RMS EVM of about 4% while using the irregular array. Considering the EVM limit shown by the red line, we can say that with both the arrays, the closeness achieved by the users is approximately the same. For the

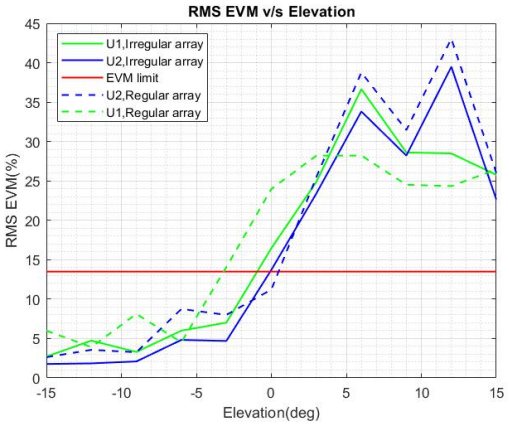

Figure 3.32: EVM v/s Elevation

irregular array, User-2 can be at an elevation angle less than 0° and for the regular array, it has to be less than 0.45°. To get more insight into the performance of users, we take a look at the precoded transmit patterns of the irregular array when User-2 has the maximum EVM. From Figure 3.33, we can calculate the interference faced by User-1 as -7.54dB and for User-2 it is -6.2dB. At the same time, for the regular array, User-2 experiences higher interference of about -5.84dB, and for User-1, it is lower and is about -10.86dB. Since users are highly correlated, the inter-user interference is more. As explained previously, the BD precoding algorithm fails to suppress the interference when users are too close to each other. This results in poor quality of the received signal, which is reflected in the constellation diagram given in Figure 3.34. The BER and EVM values for this case are summarized in Table 3.14.

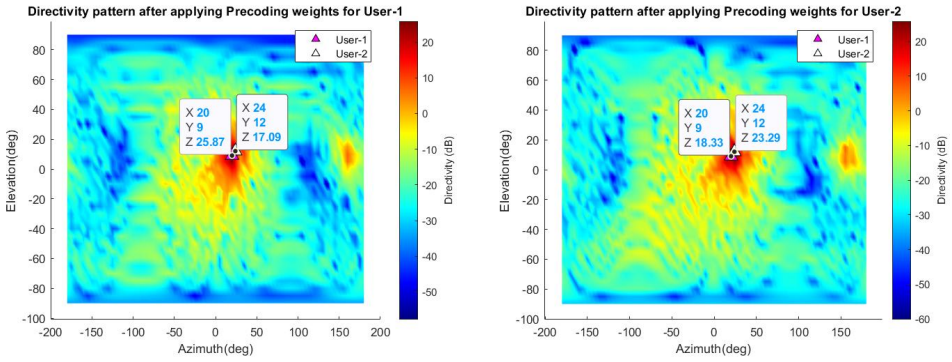

(a) (b)

Figure 3.33: Directivity pattern after applying precoding weights when User-2 is at an elevation angle 12° (a)User-1(b)User-2

User	EVM	BER
User-1	28.601%	BER=0.0009 • No. of bits=3114 • No. of errors=3
User-2	36.497%	BER=0.025 • No. of bits=3114 • No. of errors=79

Table 3.14: EVM and BER values when User-2 is at 12°(Elevation)

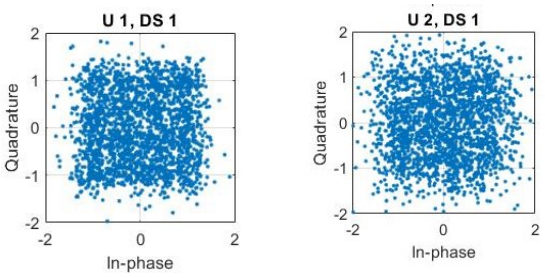

(a) (b)

Figure 3.34: Constellation diagram (a)User-1(b)User-2

3.5. Conclusion

In this chapter, we conducted a statistical analysis of the developed end-to-end MU-MIMO system model. Firstly, we discussed the specifications considered for this model, followed by a detailed review of the performance metrics- EVM and BER which were considered for evaluating the system. We performed different case studies by changing the user position(range, azimuth, and elevation) and antenna array size at the BS to investigate the impact on the performance of the users. These case studies were conducted with the model for two different BS array topologies-(i) Regular antenna array, (ii) Irregular antenna array. In the first case, we explored the effect of changing the range of User-2 and evaluating the performance of both the users. From the results of the Monte-Carlo simulations performed for both the array topologies, we found that EVM is independent of the range of the users. For both users, EVM remains almost constant with range. However, we see some random fluctuations, which could be due to the rich scattering nature of the channel.

In the second case, we varied the azimuth position of User-2 from -60° to 60° and studied the impact on EVM and BER. As User-2 moved closer towards User-1 in azimuth, we could see a deterioration in the performance of users. The EVM increased beyond the permissible EVM limits, and the BER also showed an increasing trend. This observation is due to the high spatial correlation of the users when they are closely separated and the inter-user interference increases. When the users are too close to each other, the BD precoding algorithm fails to cancel out the interference towards the unintended user. A similar observation is made in the next case when the elevation of User-2 is changed from -15° to 15° by keeping all other parameters constant. Hence, we can conclude that the spatial separation in azimuth and elevation play a major role in the performance of the users. When the users are close to each other in azimuth, by ensuring sufficient separation in the elevation plane, we can reduce the inter-user interference and vice-versa. Additionally, from the precoded patterns, we could see the impact of the higher sidelobe levels on the interference between the users. The angular separation of the users is determined by the beamwidth of the assigned beams. The minimum angular separation between the beams assigned should be greater than the azimuth and elevation beamwidth in order to have less inter-user interference.

We also investigated the impact of the array size at the BS. We see a minor impact on increasing the array size on EVM. However, the effect of increasing the number of elements at the BS solely depends on the efficiency of the precoding scheme. This is because, when we increase the array size, we have narrower beams. While this helps to have users more closely separated, if the beams are not pointed exactly to the user, we will not see an improvement in terms of EVM.

We conducted the above-mentioned cases for both regular and irregular array topology at the BS. We do not see much difference in EVM values between both the arrays on changing the range of User-2. However, for the case study conducted for changing the azimuth and elevation of User-2, we

can see the peak EVM is reduced by about 5% when the irregular array topology is used. This way, the inter-user interference is reduced. Finally, we increased the array size of the irregular array and performed the cases: changing range, azimuth, and elevation position of User-2 and evaluated the performance of the users. There is a slight reduction in the EVM when we increase the array size for the EVM versus range study. This is due to the fact that larger arrays results in improved array gain and hence better signal power is received by the users. Next, we compared the performance of both the array topologies while varying the azimuth position of User-2. Even though the interference faced by User-2 for the irregular array is less in comparison to its regular counterpart, we still see that the peak EVM is slightly higher. This is probably due to the higher contribution of other system noises, which is not known to us. In the following case, we varied the elevation of User-2 and compared the EVM curves for both the array topologies. We find that for User-2, there is an improvement of about 4% for the peak EVM. The presented results are pertaining to the One-Ring channel model, which is a rich multipath NLoS channel. With a LoS or other channel models, the performance of users would be different. Hence, we can conclude that for the given channel model, while using the irregular array topology for array size M=64, we see an improved performance of the users.

4

Conclusion And Future Scope

4.1. Conclusion

This thesis aimed to develop a simulation model for the MU-MIMO communication system for the mmWaves with a focus on multibeam arrays and beamforming at the base station. The model incorporates signal modulation, channel aspects as well as the RF aspects. Traditionally, antenna engineering and communication system design were treated as separate disciplines. However, as we move towards the multi-user communication system, there is a growing need to bridge the gap between the two disciplines. This thesis work presents a novel approach where the impact of user position, antenna parameters, and modulation is investigated on end-user performance. To the authors' knowledge, this is the first time the effect of array size and topology on the system performance is investigated. The thesis work was divided into four parts. The first part included a detailed literature survey that helped to identify a suitable channel model and system simulator to fulfill the goals of the thesis. This was followed by the development of the system model. The next part was dedicated to the statistical analysis and case study with the results obtained from the model. In the last part, the conclusions of the thesis are summarized.

A detailed literature study of existing MU-MIMO models, channel models, and system-level simulators gave us an insight into the vast possibilities to develop a communication system. Based on the complexity of the models, required inputs, etc., it was decided to use an extended version of an existing multi-user communication model in MATLAB for our study. This particular model carefully considers all the important components of the communication system, i.e. from channel coding, OFDM modulation/demodulation, antenna design, channel modeling, hybrid beamforming, precoding technique, and equalization at the receiver. The model has been adjusted for the application with different array topologies at the base station. The complete system model for multi-user scenarios and multi-beam antenna arrays at the base station has been developed. To our best knowledge, such a complete model has been presented in the literature for the first time. In this work, a downlink multi-user communication system was implemented with two users in a single cell. For the base station, we considered two different antenna array topologies: Regular and Irregular array for our study. In this model, technology like spatial multiplexing was implemented to achieve higher capacity. The model used the One-Ring channel model, which created a rich multi-path environment. Bearing in mind the power consumption and hardware complexity, hybrid beamforming architecture is chosen at the transmitter. A Joint Spatial Division Multiplexing(JSDM) is employed to obtain analog and digital precoding weights. The JSDM utilizes the generalized zero-forcing precoding technique to

efficiently cancel out the inter-user interference. At the receiver side, we consider the users are equipped with multiple antennas, and we have an all-digital receiver.

The model has been verified by simulating a simple use case scenario where the users were spatially separated, and a regular antenna array was used at the base station. In order to validate the user performance, we use EVM which has caught a lot of attention in recent research as well as the BER metric. Further, performance analysis was conducted via Monte Carlo simulations. The system performance with regular and irregular arrays has been analyzed in several case studies. Case study 1 dealt with the change of user position in the range, where we varied the range of User-2 while User-1 was fixed and plotted the RMS EVM versus range graph for both the users. It was observed that EVM is independent of the range, and hence we obtained an almost constant value when the range of User-2 was increased. The next two case studies were focused on investigating the impact of changing the azimuth and elevation position of the users. The analysis of the results has shown that spatial separation of users in azimuth and elevation has a huge impact on user performance. We kept the User-1 fixed and varied the azimuth position of User-2. As User-2 moved closer in azimuth towards User-1, there was an increase in the EVM and BER values. This behavior is as expected, since the inter-user interference increases when the users are brought close together. Apart from that, when the users are highly correlated, the BD precoding algorithm fails to efficiently cancel the inter-user interference, and also the SINR experienced by the user decreases. Hence, an effective precoding algorithm also plays a key role in end-user performance. Apart from that, we noticed the influence of sidelobe level on the interference and further on the EVM and BER. Therefore, by ensuring sufficient separation in both azimuth and elevation, we can guarantee less interference between the users.

The next case study was on increasing the number of antenna elements at the base station. There is a minor impact of the array size on the reported EVM values. A slight reduction in EVM was observed when the user position is changed in comparison to the smaller array. This is because array gain is increased when we increased the number of transmit elements from 64 to 256. Additionally, the results showed that users could be more close to each other while using the larger array due to the reduced beamwidth of the assigned beams. Increasing the array size is of an advantage only when the beam is correctly directed towards the user. Finally, the case studies were repeated for the irregular array at the base station and a comparison was drawn between the performance of the users. For M=64 antenna elements at the base station, we see about 6% reduction in the peak EVM value for User-2 for the EVM versus azimuth graph while using the irregular array. A similar observation was made for the EVM versus elevation graph, where the peak EVM for User-2 is reduced by 5%. When we increased the array size to M=256, for the EVM versus azimuth graph, we could see that the regular array performed better in terms of the reported peak EVM. Even though the interference experienced is lower while using the irregular array, EVM was still reported to be slightly higher. The reason for this anomaly is not clear. In general, from the user performance, we can conclude that both the array topologies' performance is comparable. However, the irregular array with M=64 elements has a slight improvement in terms of user performance. The presented results are completely novel and demonstrate the importance of the array size and topology on the end-user performance of the communication system.

The major challenge of this thesis was to understand and develop the end-to-end system model. An extensive study was needed to analyze the different disciplines that are involved in making the model working. Another challenge was to connect the different perspectives of antenna engineering and signal processing engineering. Apart from that, understanding the performance metric EVM and analyzing it in different case studies was not straightforward. This is because EVM is a comprehen-

sive metric that is sensitive to any noise and signal distortions. Despite these challenges, we are able to meet the goals of the thesis. Therefore, the developed system model and statistical analysis can be used to improve the existing communication system design.

4.2. Future Scope

We can consider the following areas for future scope:

- Investigation of better precoding strategies to efficiently cancel interference with less complexity can be investigated. The current generalized zero-forcing precoding fails to perform efficiently in a low SINR scenario.
- Currently, we have considered the simulations for two users and a single stream assigned to each user. A case study can further be conducted by increasing the number of users and streams, and its impact on EVM can also be explored.
- The channel model employed in the thesis considers only multipath scenarios based on the One Ring channel model. In the future, we can consider a more realistic channel simulator like QuaDRiGa, which has more flexibility in terms of environment settings.
- The effect of mutual coupling is ignored in this work. As a next step, we could study the impact of mutual coupling on end-user performance.
- An optimization can be performed for the different antenna element positions by adjusting the element spacing in the base station and study the impact on the performance of the users.

A

Definition of Coordinate System

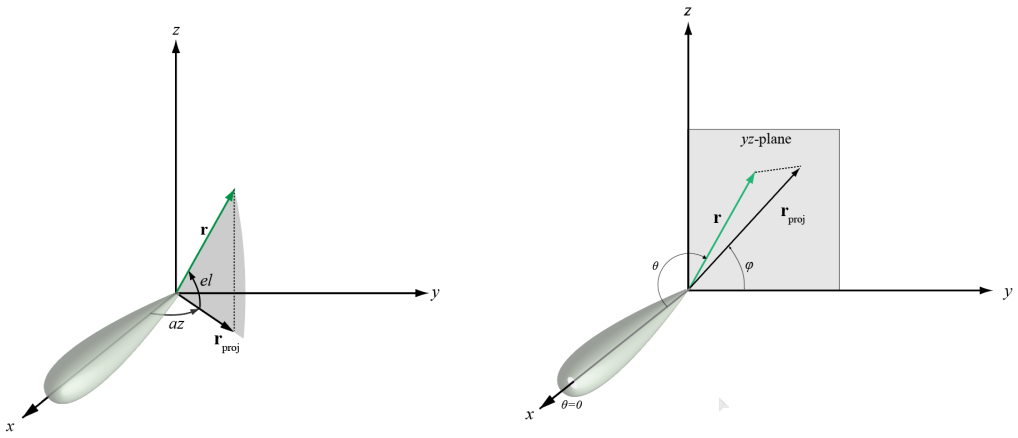

Figure A.1: Definition of spherical coordinates(adapted from [8]) (a)Azimuth and Elevation angles(b)Theta and Phi angles

Figure A.1 shows the definition of the spherical coordinates that is used in the thesis. Let us consider the vector *r* which points towards the direction of interest. The azimuth angle is the angle that *x-axis* makes with the projection of the *r* vector onto the *xy-plane*. Whereas, the elevation angle is defined as the angle that the *r* vector makes with its orthogonal projection on the *xy-plane*. We can also represent the angles in θ and ϕ. θ is the angle between the *x-axis* and the *r* vector. Angle ϕ is the angle that the positive *y-axis* makes with the projection vector of *r* onto the *yz-plane*. ϕ varies from 0 to 360 degrees and θ varies from 0 to 180 degrees.
The coordinate conversion between θ/ϕ and azimuth/elevation is given below [8]:

$$\sin el = \sin\phi \sin\theta$$

$$\tan az = \cos\phi \tan\theta$$

$$\cos\theta = \cos el \cos az$$

$$\tan\phi = \frac{\tan el}{\tan az}$$

Bibliography

[1] P.-S. Kildal and A. A. Glazunov, "OTA testing of 3G-5G devices with MIMO: From anechoic chambers to reverberation chambers and … back again?" in *2017 IEEE International Symposium on Antennas and Propagation & USNC/URSI National Radio Science Meeting*. San Diego, CA, USA: IEEE, Jul. 2017, pp. 1697–1698. [Online]. Available: http://ieeexplore.ieee.org/document/8072891/

[2] "Massive MIMO Hybrid Beamforming - MATLAB & Simulink - MathWorks Benelux." [Online]. Available: https://nl.mathworks.com/help/phased/ug/massive-mimo-hybrid-beamforming.html

[3] "Hybrid MIMO Beamforming with QSHB and HBPS Algorithms - MATLAB & Simulink - MathWorks Nordic." [Online]. Available: https://se.mathworks.com/help/phased/ug/hybrid-mimo-beamforming-with-qshb-and-hbps-algorithms.html#d122e34085

[4] "mmWave communication enabling techniques for 5G wireless systems: A link level perspective | Elsevier Enhanced Reader."

[5] W. Tan, W. Huang, X. Yang, Z. Shi, W. Liu, and L. Fan, "Multiuser precoding scheme and achievable rate analysis for massive MIMO system," *EURASIP Journal on Wireless Communications and Networking*, vol. 2018, no. 1, p. 210, Aug. 2018. [Online]. Available: https://doi.org/10.1186/s13638-018-1223-1

[6] D.-S. Shiu, G. Foschini, M. Gans, and J. Kahn, "Fading correlation and its effect on the capacity of multielement antenna systems," *IEEE Transactions on Communications*, vol. 48, no. 3, pp. 502–513, Mar. 2000, conference Name: IEEE Transactions on Communications.

[7] "What is EVM? - everything RF." [Online]. Available: https://www.everythingrf.com/community/what-is-evm

[8] "Spherical Coordinates - MATLAB & Simulink - MathWorks Benelux." [Online]. Available: https://nl.mathworks.com/help/phased/ug/spherical-coordinates.html

[9] "Technical Specification Group Radio Access Network; NR; User Equipment (UE) Radio Transmission and Reception," 2018.

[10] C. Sun, X. Gao, S. Jin, M. Matthaiou, Z. Ding, and C. Xiao, "Beam Division Multiple Access Transmission for Massive MIMO Communications," *IEEE Transactions on Communications*, vol. 63, no. 6, pp. 2170–2184, Jun. 2015, conference Name: IEEE Transactions on Communications.

[11] J. Kelner and C. Ziółkowski, "Interference in multi-beam antenna system of 5G network," *International Journal of Electronics and Telecommunications*, vol. 66, pp. 17–23, Feb. 2020.

[12] C. Wang, "Adaptive downlink multi-user MIMO wireless systems," 2007.

[13] T. Chapman, E. Larsson, P. von Wrycza, E. Dahlman, S. Parkvall, and J. Sköld, "Chapter 11 - Multi-antenna transmission," in *HSPA Evolution*, T. Chapman, E. Larsson, P. von Wrycza, E. Dahlman, S. Parkvall, and J. Sköld, Eds. Oxford: Academic Press, Jan. 2015, pp. 235–306. [Online]. Available: https://www.sciencedirect.com/science/article/pii/B9780080999692000119

[14] A. Zaidi, F. Athley, J. Medbo, U. Gustavsson, G. Durisi, and X. Chen, “Chapter 7 - Multiantenna Techniques,” in *5G Physical Layer*, A. Zaidi, F. Athley, J. Medbo, U. Gustavsson, G. Durisi, and X. Chen, Eds. Academic Press, Jan. 2018, pp. 199–252. [Online]. Available: https://www.sciencedirect.com/science/article/pii/B9780128145784000126

[15] accton_en, “The Emergence of 5G mmWave.” [Online]. Available: https://www.accton.com/Technology-Brief/the-emergence-of-5g-mmwave/

[16] M. Shehata, A. Mokh, M. Crussière, M. Hélard, and P. Pajusco, “On the Equivalence of Hybrid Beamforming to Full Digital Zero Forcing in mmWave MIMO,” in *26th Internatinal Conference on Telecommunication (ICT 2019)*, Hanoi, Vietnam, Apr. 2019. [Online]. Available: https://hal.archives-ouvertes.fr/hal-01976833

[17] R. v. Nee and R. Prasad, *OFDM for Wireless Multimedia Communications*. Artech House, 2000, google-Books-ID: 1gBTAAAAMAAJ.

[18] M. Esslaoui and M. Essaaidi, “Performance of Multiuser MIMO-OFDM downlink system with ZF-BF and MMSE-BF linear precoding,” vol. 3, no. 4, p. 7, 2013.

[19] H. Määttänen, “MIMO-OFDM.”

[20] G. Oliveri, G. Gottardi, and A. Massa, “A New Meta-Paradigm for the Synthesis of Antenna Arrays for Future Wireless Communications,” *IEEE Transactions on Antennas and Propagation*, vol. 67, no. 6, pp. 3774–3788, Jun. 2019. [Online]. Available: https://ieeexplore.ieee.org/document/8672129/

[21] Y. Qi, G. Yang, L. Liu, J. Fan, A. Orlandi, H. Kong, W. Yu, and Z. Yang, “5G Over-the-Air Measurement Challenges: Overview,” *IEEE Transactions on Electromagnetic Compatibility*, vol. 59, no. 6, pp. 1661–1670, Dec. 2017. [Online]. Available: http://ieeexplore.ieee.org/document/7936575/

[22] H. Chung, Q. Ma, Y. Yin, L. Gao, and G. M. Rebeiz, “A 25-29 GHz 64-Element Dual-Polarized/Dual-Beam Small-Cell with 45 dBm 400 MHz 5GNR Operation and High Spectral Purity,” in *2020 IEEE/MTT-S International Microwave Symposium (IMS)*. Los Angeles, CA, USA: IEEE, Aug. 2020, pp. 1267–1270. [Online]. Available: https://ieeexplore.ieee.org/document/9223975/

[23] Y. Yin, T. Phelps, B. Ustundag, K. Kibaroglu, M. Sayginer, and G. M. Rebeiz, “A 1 Gbps 3.5-4.75 km Communication Link Based on a 5G 28 GHz 8×8 Phased-Array,” in *2019 IEEE International Symposium on Phased Array System & Technology (PAST)*. Waltham, MA, USA: IEEE, Oct. 2019, pp. 1–4. [Online]. Available: https://ieeexplore.ieee.org/document/9020881/

[24] S. Spira, R. S. Thoma, and M. Hein, “A Multi-Beam Direction- and Polarization-Agile mm-Wave Front-End for 5G Communications,” in *2019 12th German Microwave Conference (GeMiC)*. Stuttgart, Germany: IEEE, Mar. 2019, pp. 71–74. [Online]. Available: https://ieeexplore.ieee.org/document/8698147/

[25] A. Glazunov, “Impact of Deficient Array Antenna Elements on Downlink Massive MIMO Performance in RIMP and Random-LOS Channels,” in *12th European Conference on Antennas and Propagation (EuCAP 2018)*. London, UK: Institution of Engineering and Technology, 2018, pp. 528 (4 pp.)–528 (4 pp.). [Online]. Available: https://digital-library.theiet.org/content/conferences/10.1049/cp.2018.0887

[26] P. Gkonis, T. Panagiotis, and D. Kaklamani, “A Comprehensive Study on Simulation Techniques for 5G Networks: State of the Art Results, Analysis, and Future Challenges,” *Electronics*, vol. 9, p. 468, Mar. 2020.

[27] C.-X. Wang, J. Bian, J. Sun, W. Zhang, and M. Zhang, “A Survey of 5G Channel Measurements and Models,” *IEEE Communications Surveys & Tutorials*, vol. 20, no. 4, pp. 3142–3168, 2018. [Online]. Available: https://ieeexplore.ieee.org/document/8424015/

[28] S. Jaeckel, L. Raschkowski, K. Borner, and L. Thiele, “QuaDRiGa: A 3-D Multi-Cell Channel Model With Time Evolution for Enabling Virtual Field Trials,” *IEEE Transactions on Antennas and Propagation*, vol. 62, no. 6, pp. 3242–3256, Jun. 2014. [Online]. Available: http://ieeexplore.ieee.org/document/6758357/

[29] A. M. Pessoa, I. M. Guerreiro, C. F. M. E. Silva, T. F. Maciel, D. A. Sousa, D. C. Moreira, and F. R. P. Cavalcanti, “A Stochastic Channel Model With Dual Mobility for 5G Massive Networks,” *IEEE Access*, vol. 7, pp. 149 971–149 987, 2019. [Online]. Available: https://ieeexplore.ieee.org/document/8868161/

[30] D. Baum, J. Hansen, G. Galdo, M. Milojevic, J. Salo, and P. Kyosti, “An Interim Channel Model for Beyond-3G Systems Extending the 3GPP Spatial Channel Model (SCM),” in *2005 IEEE 61st Vehicular Technology Conference*, vol. 5. Stockholm, Sweden: IEEE, 2005, pp. 3132–3136. [Online]. Available: http://ieeexplore.ieee.org/document/1543924/

[31] J. Joung, E. Kurniawan, and S. Sun, “Channel Correlation Modeling and its Application to Massive MIMO Channel Feedback Reduction,” *IEEE Transactions on Vehicular Technology*, pp. 1–1, 2016. [Online]. Available: http://ieeexplore.ieee.org/document/7534862/

[32] P. Petrus, J. Reed, and T. Rappaport, “Geometrical-based statistical macrocell channel model for mobile environments,” *IEEE Transactions on Communications*, vol. 50, no. 3, pp. 495–502, Mar. 2002. [Online]. Available: http://ieeexplore.ieee.org/document/990911/

[33] A. Burr, “Capacity bounds and estimates for the finite scatterers MIMO wireless channel,” *IEEE Journal on Selected Areas in Communications*, vol. 21, no. 5, pp. 812–818, Jun. 2003. [Online]. Available: http://ieeexplore.ieee.org/document/1203166/

[34] S. Wu, C.-X. Wang, E.-H. M. Aggoune, and M. M. Alwakeel, “A novel Kronecker-based stochastic model for massive MIMO channels,” in *2015 IEEE/CIC International Conference on Communications in China (ICCC)*. Shenzhen, China: IEEE, Nov. 2015, pp. 1–6. [Online]. Available: http://ieeexplore.ieee.org/document/7448642/

[35] N. Anselmi, G. Gottardi, P. Rocca, G. Oliveri, and A. Massa, “Unconventional M-MIMO Phased Array Design for 5G Wireless Systems,” in *2019 IEEE International Symposium on Phased Array System & Technology (PAST)*. Waltham, MA, USA: IEEE, Oct. 2019, pp. 1–3. [Online]. Available: https://ieeexplore.ieee.org/document/9020766/

[36] T. S. Rappaport, S. Sun, and M. Shafi, “Investigation and Comparison of 3GPP and NYUSIM Channel Models for 5G Wireless Communications,” in *2017 IEEE 86th Vehicular Technology Conference (VTC-Fall)*. Toronto, ON: IEEE, Sep. 2017, pp. 1–5. [Online]. Available: http://ieeexplore.ieee.org/document/8287877/

[37] S. Sun, G. R. MacCartney, and T. S. Rappaport, “A novel millimeter-wave channel simulator and applications for 5G wireless communications,” in *2017 IEEE International Conference on Communications (ICC)*. Paris, France: IEEE, May 2017, pp. 1–7. [Online]. Available: http://ieeexplore.ieee.org/document/7996792/

[38] M. E. Hassan, A. E. Falou, and C. Langlais, “Performance assessment of linear precoding for multi-user massive MIMO systems on a realistic 5G mmWave channel,” in *2018 IEEE Middle East and North Africa Communications Conference (MENACOMM)*. Jounieh: IEEE, Apr. 2018, pp. 1–5. [Online]. Available: https://ieeexplore.ieee.org/document/8371025/

[39] M. Mbeutcha, W. Fan, J. Hejsclbaek, and G. F. Pedersen, “Evaluation of massive MIMO systems using time-reversal beamforming technique,” in *2016 IEEE 27th Annual International Symposium on Personal, Indoor, and Mobile Radio Communications (PIMRC)*. Valencia: IEEE, Sep. 2016, pp. 1–6. [Online]. Available: http://ieeexplore.ieee.org/document/7794571/

[40] J. Weng, X. Tu, Z. Lai, S. Salous, and J. Zhang, “Indoor Massive MIMO Channel Modelling Using Ray-Launching Simulation,” *International Journal of Antennas and Propagation*, vol. 2014, p. e279380, Aug. 2014, publisher: Hindawi. [Online]. Available: https://www.hindawi.com/journals/ijap/2014/279380/

[41] L. Raschkowski, P. Kyösti, K. Kusume, T. Jämsä, V. Nurmela, A. Karttunen, A. Roivainen, T. Imai, J. Järveläinen, J. Medbo, J. Vihriälä, J. Meinilä, K. Haneda, V. Hovinen, J. Ylitalo, N. Omaki, A. Hekkala, R. Weiler, and M. Peter, *METIS Channel Models (D1.4)*, Jul. 2015.

[42] F. Hossain, T. Geok, T. Rahman, M. Hindia, K. Dimyati, S. Ahmed, C. Tso, and N. Z. Abd Rahman, “An Efficient 3-D Ray Tracing Method: Prediction of Indoor Radio Propagation at 28 GHz in 5G Network,” *PLoS ONE*, vol. 8, p. 286, Mar. 2019.

[43] V. Degli-Esposti, F. Fuschini, E. M. Vitucci, M. Barbiroli, M. Zoli, L. Tian, X. Yin, D. A. Dupleich, R. Muller, C. Schneider, and R. S. Thoma, “Ray-Tracing-Based mm-Wave Beamforming Assessment,” *IEEE Access*, vol. 2, pp. 1314–1325, 2014. [Online]. Available: http://ieeexplore.ieee.org/document/6942178/

[44] Y. Aslan, J. Puskely, A. Roederer, and A. Yarovoy, “Performance Comparison of Single- and Multi-Lobe Antenna Arrays in 5G Urban Outdoor Environments at mm-Waves via Intelligent Ray Tracing,” in *2020 14th European Conference on Antennas and Propagation (EuCAP)*. Copenhagen, Denmark: IEEE, Mar. 2020, pp. 1–5. [Online]. Available: https://ieeexplore.ieee.org/document/9135263/

[45] J. B. info@jbachmann.net, “QuaDRiGa.” [Online]. Available: https://quadriga-channel-model.de/

[46] C.-K. Jao, C.-Y. Wang, T.-Y. Yeh, C.-C. Tsai, L.-C. Lo, J.-H. Chen, W.-C. Pao, and W.-H. Sheen, “WiSE: A System-Level Simulator for 5G Mobile Networks,” *IEEE Wireless Communications*, vol. 25, no. 2, pp. 4–7, Apr. 2018. [Online]. Available: https://ieeexplore.ieee.org/document/8352614/

[47] M. Liu, P. Ren, Q. Du, W. Ou, X. Xiong, and G. Li, “Design of system-level simulation platform for 5G networks,” in *2016 IEEE/CIC International Conference on Communications in China (ICCC)*. Chengdu, China: IEEE, Jul. 2016, pp. 1–6. [Online]. Available: http://ieeexplore.ieee.org/document/7636796/

[48] M. Mezzavilla, M. Zhang, M. Polese, R. Ford, S. Dutta, S. Rangan, and M. Zorzi, “End-to-End Simulation of 5G mmWave Networks,” *IEEE Communications Surveys & Tutorials*, vol. 20, no. 3, pp. 2237–2263, 2018. [Online]. Available: https://ieeexplore.ieee.org/document/8344116/

[49] M. K. Müller, F. Ademaj, T. Dittrich, A. Fastenbauer, B. Ramos Elbal, A. Nabavi, L. Nagel, S. Schwarz, and M. Rupp, “Flexible multi-node simulation of cellular mobile

communications: the Vienna 5G System Level Simulator," *EURASIP Journal on Wireless Communications and Networking*, vol. 2018, no. 1, p. 227, Sep. 2018. [Online]. Available: https://doi.org/10.1186/s13638-018-1238-7

[50] N. Amani, H. Wymeersch, U. Johannsen, A. B. Smolders, M. V. Ivashina, and R. Maaskant, "Multi-Panel Sparse Base Station Design With Physical Antenna Effects in Massive MU-MIMO," *IEEE Transactions on Vehicular Technology*, vol. 69, no. 6, pp. 6500–6510, Jun. 2020. [Online]. Available: https://ieeexplore.ieee.org/document/9072598/

[51] ——, "Towards a Generic Model for MU-MIMO Analysis Including Mutual Coupling and Multi-path Effects," in *2019 13th European Conference on Antennas and Propagation (EuCAP)*, Mar. 2019, pp. 1–4.

[52] N. Amani, R. Maaskant, A. Glazunov, and M. Ivashina, "Network Model of a 5G MIMO Base Station Antenna in a Downlink Multi-User Scenario," in *12th European Conference on Antennas and Propagation (EuCAP 2018)*. London, UK: Institution of Engineering and Technology, 2018, pp. 908 (5 pp.)–908 (5 pp.). [Online]. Available: https://digital-library.theiet.org/content/conferences/10.1049/cp.2018.1267

[53] "5G Toolbox." [Online]. Available: https://se.mathworks.com/products/5g.html

[54] Da-Shan Shiu, G. Foschini, M. Gans, and J. Kahn, "Fading correlation and its effect on the capacity of multielement antenna systems," *IEEE Transactions on Communications*, vol. 48, no. 3, pp. 502–513, Mar. 2000. [Online]. Available: http://ieeexplore.ieee.org/document/837052/

[55] P. Kyösti, J. Meinilä, L. Hentila, X. Zhao, T. Jämsä, C. Schneider, M. Narandzic, M. Milojević, A. Hong, J. Ylitalo, V.-M. Holappa, M. Alatossava, R. Bultitude, Y. Jong, and T. Rautiainen, "WINNER II channel models," *IST-4-027756 WINNER II D1.1.2 V1.2*, Feb. 2008.

[56] "802.11ac Multi-User MIMO Precoding with WINNER II Channel Model - MATLAB & Simulink - MathWorks Nordic." [Online]. Available: https://se.mathworks.com/help/comm/ug/802-11ac-multi-user-mimo-precoding-with-winner-ii-channel-model.html#WINNERVHTMUMIMOExample-18

[57] "MIMO-OFDM Precoding with Phased Arrays - MATLAB & Simulink - MathWorks Nordic." [Online]. Available: https://se.mathworks.com/help/comm/ug/mimo-ofdm-precoding-with-phased-arrays.html

[58] A. F. Molisch, V. V. Ratnam, S. Han, Z. Li, S. L. H. Nguyen, L. Li, and K. Haneda, "Hybrid Beamforming for Massive MIMO: A Survey," *IEEE Communications Magazine*, vol. 55, no. 9, pp. 134–141, Sep. 2017, conference Name: IEEE Communications Magazine.

[59] A. Adhikary, E. A. Safadi, M. Samimi, R. Wang, G. Caire, T. S. Rappaport, and A. F. Molisch, "Joint Spatial Division and Multiplexing for mm-Wave Channels," *arXiv:1312.2045 [cs, math]*, May 2014, arXiv: 1312.2045. [Online]. Available: http://arxiv.org/abs/1312.2045

[60] J. Salz and J. Winters, "Effect of fading correlation on adaptive arrays in digital wireless communications," in *Proceedings of ICC '93 - IEEE International Conference on Communications*, vol. 3, May 1993, pp. 1768–1774 vol.3.

[61] W. Lee, "Effects on Correlation Between Two Mobile Radio Base-Station Antennas," *IEEE Transactions on Communications*, vol. 21, no. 11, pp. 1214–1224, Nov. 1973, conference Name: IEEE Transactions on Communications.

[62] P. Sudarshan, N. B. Mehta, A. F. Molisch, and J. Zhang, “Channel Statistics-Based RF Pre-Processing with Antenna Selection,” *IEEE Transactions on Wireless Communications*, vol. 5, no. 12, pp. 3501–3511, Dec. 2006, conference Name: IEEE Transactions on Wireless Communications.

[63] X. Zhang, A. Molisch, and S.-Y. Kung, “Variable-phase-shift-based RF-baseband codesign for MIMO antenna selection,” *Signal Processing, IEEE Transactions on*, vol. 53, pp. 4091–4103, Dec. 2005.

[64] Z. Li, S. Han, and A. F. Molisch, “Hybrid beamforming design for millimeter-wave multi-user massive MIMO downlink,” in *2016 IEEE International Conference on Communications (ICC)*, May 2016, pp. 1–6, iSSN: 1938-1883.

[65] J. Nam, A. Adhikary, J.-Y. Ahn, and G. Caire, “Joint Spatial Division and Multiplexing: Opportunistic Beamforming, User Grouping and Simplified Downlink Scheduling,” *IEEE Journal of Selected Topics in Signal Processing*, vol. 8, no. 5, pp. 876–890, Oct. 2014, conference Name: IEEE Journal of Selected Topics in Signal Processing.

[66] A. F. Molisch, *Wireless Communications, 2nd Edition*. Wiley-IEEE Press, 2011.

[67] K. Mittal, S. Pathania, P. Reddy, and D. Rawal, “Channel State Information feedback overhead reduction using Arithmetic coding in massive MIMO systems,” in *2016 3rd International Conference on Signal Processing and Integrated Networks (SPIN)*, Feb. 2016, pp. 328–331.

[68] A. Adhikary, J. Nam, J.-Y. Ahn, and G. Caire, “Joint Spatial Division and Multiplexing—The Large-Scale Array Regime,” *IEEE Transactions on Information Theory*, vol. 59, no. 10, pp. 6441–6463, Oct. 2013, conference Name: IEEE Transactions on Information Theory.

[69] T. Lo, “Maximum ratio transmission,” *IEEE Transactions on Communications*, vol. 47, no. 10, pp. 1458–1461, Oct. 1999, conference Name: IEEE Transactions on Communications.

[70] M. Joham, W. Utschick, and J. Nossek, “Linear transmit processing in MIMO communications systems,” *IEEE Transactions on Signal Processing*, vol. 53, no. 8, pp. 2700–2712, Aug. 2005, conference Name: IEEE Transactions on Signal Processing.

[71] B. Bandemer, M. Haardt, and S. Visuri, “Linear MMSE Multi-User MIMO Downlink Precoding for Users with Multiple Antennas,” in *2006 IEEE 17th International Symposium on Personal, Indoor and Mobile Radio Communications*, Sep. 2006, pp. 1–5, iSSN: 2166-9589.

[72] Q. Spencer, A. Swindlehurst, and M. Haardt, “Zero-Forcing Methods for Downlink Spatial Multiplexing in Multiuser MIMO Channels,” *Signal Processing, IEEE Transactions on*, vol. 52, pp. 461–471, Mar. 2004.

[73] D. A. Patil and M. Bengtsson, “Block Diagonalization Based Beamforming,” p. 122.

[74] R. A. Shafik, M. S. Rahman, and A. R. Islam, “On the Extended Relationships Among EVM, BER and SNR as Performance Metrics,” in *2006 International Conference on Electrical and Computer Engineering*, Dec. 2006, pp. 408–411.

[75] M. E. Leinonen, M. Jokinen, N. Tervo, O. Kursu, and A. Parssinen, “System EVM Characterization and Coverage Area Estimation of 5G Directive mmW Links,” *IEEE Transactions on Microwave Theory and Techniques*, vol. 67, no. 12, pp. 5282–5295, Dec. 2019. [Online]. Available: https://ieeexplore.ieee.org/document/8935494/

[76] E. Adegoke, E. Kampert, and M. Higgins, “Channel Modelling and Over-the-Air Signal Quality at 3.5 GHz for 5G New Radio,” *IEEE Access*, vol. 9, pp. 11 183–11 193, Jan. 2021.

[77] M. E. Leinonen, N. Tervo, M. Jokinen, O. Kursu, and A. Pärssinen, “5G mm-Wave Link Range Estimation Based on Over-the-Air Measured System EVM Performance,” in *2019 IEEE MTT-S International Microwave Symposium (IMS)*, Jun. 2019, pp. 476–479, iSSN: 2576-7216.

[78] H. Wang and H. Zhao, “EVM performance evaluation of array channels’ amplitude and phase errors for DBF phased array antennas,” in *2010 IEEE International Symposium on Phased Array Systems and Technology*, Oct. 2010, pp. 332–334.

[79] W. Boukley Hasan, A. Doufexi, G. Oikonomou, and M. Beach, “EVM Prediction for Massive MIMO,” Sep. 2019, pp. 1–7.

[80] M. Mckinley, K. Remley, M. Myslinski, J. Kenney, D. Schreurs, and B. Nauwelaers, “EVM calculation for broadband modulated signals,” Jan. 2004.

[81] P. Harris, W. B. Hasan, S. Malkowsky, J. Vieira, S. Zhang, M. Beach, L. Liu, E. Mellios, A. Nix, S. Armour, A. Doufexi, K. Nieman, and N. Kundargi, “Serving 22 Users in Real-Time with a 128-Antenna Massive MIMO Testbed,” in *2016 IEEE International Workshop on Signal Processing Systems (SiPS)*, Oct. 2016, pp. 266–272, iSSN: 2374-7390.

[82] E. Björnson, J. Hoydis, M. Kountouris, and M. Debbah, “Massive MIMO Systems With Non-Ideal Hardware: Energy Efficiency, Estimation, and Capacity Limits,” *IEEE Transactions on Information Theory*, vol. 60, no. 11, pp. 7112–7139, Nov. 2014, conference Name: IEEE Transactions on Information Theory.

[83] Y. Aslan, S. Salman, J. Puskely, A. Roederer, and A. Yarovoy, “5G Multi-User System Simulations in Line-of-Sight With Space-Tapered Cellular Base Station Phased Arrays,” p. 6, 2019.

[84] U. Gustavsson, C. Sanchez, T. Eriksson, F. Athley, G. Durisi, P. Landin, K. Hausmair, and C. Fager, “On the Impact of Hardware Impairments on Massive MIMO,” Nov. 2014.

[85] M. Viganó, G. Toso, C. Gerard, M. Cyril, and I. Lager, “Sunflower Array Antenna with Adjustable Density Taper,” *International Journal of Antennas and Propagation*, vol. 2009, Feb. 2009.